International Journal of Fatigue 159 (2022) 106728

Contents lists available at ScienceDirect

International Journal of Fatigue

journal homepage: www.elsevier.com/locate/ijfatigue

Multiaxial fatigue life assessment of 304 austenitic stainless steel with a novel energy-based criterion

Shun Yang [a,b], Jingyu Sun [c,*]

[a] School of Energy and Power Engineering, Beihang University, Beijing 100083, China
[b] Collaborative Innovation Center for Advanced Aero-engine, China
[c] State Key Laboratory of Nonlinear Mechanics (LNM), Institute of Mechanics, Chinese Academy of Sciences, Beijing, 100190, China

ARTICLE INFO

Keywords:
Multiaxial fatigue
Loading path
Energy weight coefficient
Non-proportionality
SS304

ABSTRACT

A novel energy-based multiaxial fatigue criterion was proposed considering the effect of normal strain energy and shear strain energy. The difference of contributions of both the normal strain energy and shear strain energy on the failure of materials was identified by introducing the stress-path-dependent energy weight coefficient. A newly defined non-proportionality based on the stable hysteresis loops was introduced to the criterion considering the non-proportionality additional hardening behavior. Most of the coefficients can be determined by the monotonic tensile test which gives more opportunities for the applicability and feasibility of the new criterion in engineering practice. The performance of the new criterion was approved by comparing the predicted and tested life of SS304 under various multiaxial loading paths.

1. Introduction

It has been an agreement that most of the practical components in service in the engineering field are characterized with complex structural features and subjected to multiaxial fatigue loads. Multiaxial fatigue is of great engineering significance in the field of service life prediction, structural safety assessment and structural optimization design [1,2].

Basically, the multiaxial fatigue life prediction process of elastoplastic materials is shown in Fig. 1. Monotonic, uniaxial cyclic and multiaxial cyclic mechanical tests are preferentially carried out to provide necessary mechanical parameters to materials' elastoplastic finite element calculation and multiaxial fatigue criteria. Then applying the elastoplastic finite element calculated stress/strain to specified multiaxial fatigue criterion gives predicted fatigue life, which come back and further compare with the test results to verify the proposed criterion.

Since the elastoplastic calculation has reached perfection, a more reasonable and accurate multiaxial criterion is still pending. Generally, the multiaxial fatigue criteria can be divided into four categories: (i) stress-based criteria (Findley criterion [3]); (ii) strain-based criteria (Brown Miller criterion or BM criterion [4], Wang Brown criterion or WB criterion [5], Li criterion [6], Ince Glinka criterion or IG criterion [7,8], Zhong–Wang–Wei criterion or ZWW criterion [9,10]); (iii) stress/strain-based criteria (Fatemi Socie criterion [11]); (iv) energy-based criteria (Smith Waston Topper criterion or SWT criterion [12,13], Ellyin criterion [14], Liu criteria [15], Chu Conle Bonnen criterion or CCB criterion [16], Chen criterion [17], Modified SWT criterion or MSWT criterion [18–20], Varvani criterion [21–23], Lazzarin criterion [24–26], Lagoda criterion [27–30], Zhu criterion [31], Branco criterion [32–34], Liu criterion [35,36]). This study is not intended to review the development of multiaxial fatigue criteria, but systematically classify these criteria, so as to compare them and clarify their characteristics. The detailed expressions are presented in Table 1 and more investigations are available in [7,37–40].

In the early years, the multiaxial criterion developed was to take the stress, strain, or homogeneous combination of them as the only indicator to determine the multiaxial damage. The commonly used stress components are the maximum normal stress (FS criterion [11]), the maximum value of the homogeneous combination of normal stress and shear stress (Findley criterion [3]), the maximum shear strain (WB and BM criteria [4,5]), the maximum value of the homogeneous combination of normal strain and shear strain (Li and IG criteria [6–8]), as well as the maximum normal strain on the π-plane (ZWW criterion [9]). However, [7,35,40] indicated that the application of specified stress or strain component as a damage indicator usually leads to an unsatisfied life prediction or an unreasonable failure mechanism. Therefore, the energy based multiaxial criteria, which considered contributions of both stress and strain were further proposed.

The SWT model [12] was firstly developed to consider the effect of mean stress on fatigue performance. Bannantine and Socie [13] further

* Corresponding author.
E-mail address: sunjingyu@imech.ac.cn (J. Sun).

https://doi.org/10.1016/j.ijfatigue.2022.106728
Received 9 September 2021; Received in revised form 8 December 2021; Accepted 6 January 2022
Available online 4 February 2022

Nomenclature

α	Energy weight coefficient
α_{ij}	Deviatoric part of back stress tensor
α_{ij}^{k}	Back stress
b	Fatigue strength exponent
b'	Shear fatigue strength exponent
β_{ij}	Radius of the nonhardening surface
c	Fatigue ductility exponent
c'	Shear fatigue ductility exponent
C_{ijkl}	Elastic constant tensor
E	Young's modulus
$\hat{E}$	Normal strain energy
f	Plastic potential function
g	Plastic strain proposed by Chaboche
G	Shear modulus
$\hat{G}$	Shear strain energy
h^k, r^k	State variables
$H(\cdot)$	Heaviside step function
$I_{\Gamma'}$, $I_{\Gamma''}$	The moment of inertia
κ	Non-proportional cyclic hardening factor
κ_{F}	Material dependent parameter
κ_{BM}	Material dependent parameter
κ_{FS}	Material dependent parameter
κ_{WB}	Material dependent parameter
K'	Cyclic strain hardening coefficient
$\dot{\lambda}$	Undetermined scalar multiplier
m_1, m_2	Undetermined coefficients
$\hat{M}$	Total strain energy
n'	Cyclic strain hardening exponent
N_{f}	Fatigue life
$\dot{p}$	Increment in effective plastic strain
P	Number of paths
q	Center of the nonhardening surface
σ_{b}	Ultimate stress
σ_{y}	Yield stress
$\varepsilon_{\mathrm{f}}'$	Fatigue ductility coefficient
ε_{ij}	Total strain tensor
$\varepsilon_{ij}^{\mathrm{e}}$, $\varepsilon_{ij}^{\mathrm{p}}$	Elastic and plastic strain tensors
γ_{f}'	Shear fatigue ductility coefficient
σ_{f}'	Fatigue strength coefficient
σ_{ij}	Stress tensor
s_{ij}	Deviatoric part of stress tensor
τ_{f}'	Shear fatigue strength coefficient
$\Delta\varepsilon$	Normal strain range
$\Delta\gamma$	Shear strain range
$\Delta\sigma$	Normal stress range
$\Delta\tau$	Shear stress range
ν_{e}, ν_{p}	Elastic and plastic Poisson's ratios
ξ	Torsion–tension energy ratio
$\boldsymbol{\Phi}$	Non-proportionality
Y	Size of yield surface
Y_0	Yield stress for proportional loading
$Y_{\Delta\mathrm{np}}$	Non-proportional hardening
$Y_{\Delta\mathrm{nps}}$	Saturated value of $Y_{\Delta\mathrm{np}}$
i, j, k, l	Variable indicator

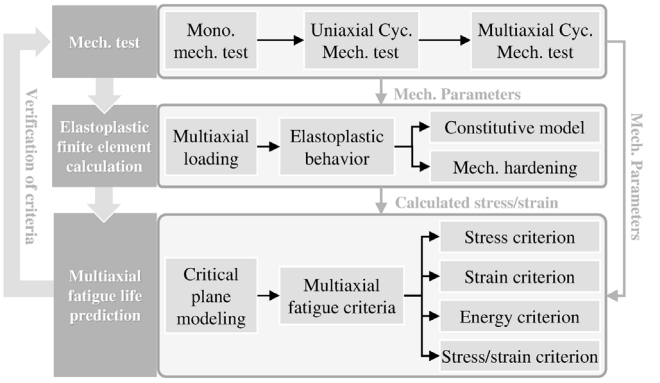

Fig. 1. Multiaxial fatigue life prediction process of elastoplastic materials based on critical plane method.

introduced the SWT model into multiaxial fatigue life prediction based on the concept of critical plane, which is almost the earliest energy criterion. In earlier studies, Ellyin [14] made a great contribution to the evaluation of multiaxial fatigue performance of metallic materials by proposing a master life curve, which designated the driving energy as a multiaxial damage indicator. As reported, the driving energy contains two components, namely the elastic and plastic energy calculated from the cyclic stress–strain curve. Liu [15] also considered the shear strain energy ($\Delta\tau\Delta\gamma$), indicating that the damage of material under multiaxial fatigue loading is the combination of both normal strain energy ($\Delta\sigma_{\mathrm{n}}\Delta\varepsilon_{\mathrm{n}}$) and shear strain energy. Since the failure modes of materials with various mechanical properties are quite different, Liu suggested the normal strain energy and shear strain energy dominated criteria, respectively, which are more reasonable on modeling materials with the significant difference in mechanical properties. Subsequently, Chen [17] proposed a criterion similar to Liu, but the difference is that the Chen criterion used the maximum shear strain amplitude ($\Delta\gamma_{\max}$) as the damage indicator. Meanwhile, the CCB criterion [16] considered that both the normal strain energy and shear strain energy work together to degrade the multiaxial fatigue performance. Furthermore, the modified SWT (MSWT) criterion [18–20] developed by Jiang et al. considered the difference of contribution of shear strain energy and normal strain energy to material failure. Accordingly, an adjustable parameter a was introduced. The Varvani criterion [21–23] was similar to the Chen criterion and Liu criteria. Although it did not introduce adjustable parameters like the MSWT criterion, the difference between the normal strain energy and shear strain energy was considered by dimensionless treatment of them. To find strategies for taking the stress concentration into account with respect to the notch features, Lazzarin [24–26] introduced the stress concentration factors under uniaxial and bending loading conditions into the normal and shear strain component respectively. Correlation of the total strain energy with fatigue life demonstrated a linear relationship. More criteria proposed by Lagoda [27–30], Zhu [31], Branco [32–34] and Lu [35,36] are available in Table 1, which also considered the shear strain energy and the normal strain energy respectively and introduced adjustable parameters to distinguish the different contributions of them to material failure under multiaxial fatigue loads. As it was reported in these investigations, these criteria successfully predicted the multiaxial fatigue performance of various materials regardless of engineering applicability and feasibility. Moreover, a considerable amount of studies on multiaxial fatigue characterized the loading path during the tests based on strain component ($\gamma/\sqrt{3}$ vs. ε). Since most of the multiaxial fatigue tests reported in studies carried out with strain controlling mode, which may fail to obtain the stress response of materials. Therefore, it is reasonable to characterize the loading path based on the stress

Table 1
Multiaxial fatigue criteria.

(Part I)			
Criteria	Expressions		References
Stress	Findley	$\left(\frac{\Delta\tau}{2}+\kappa_F\sigma_n\right)_{max}=\frac{\tau_f'}{G}(2N_f)^{b'}$	[3]
Strain	BM	$\frac{\gamma_{max}}{2}+\kappa_{BM}\Delta\varepsilon_n=A\frac{\sigma_f'}{E}(2N_f)^b+B\varepsilon_f'(2N_f)^c$	[4]
	WB	$\frac{\Delta\gamma_{max}}{2}+\kappa_{WB}\frac{\Delta\varepsilon_n}{2}=A\frac{\sigma_f'-2\sigma_{n,mean}}{E}(2N_f)^b+B\varepsilon_f'(2N_f)^c$	[5]
	Li	$\frac{\Delta\varepsilon_{eq}^*}{2}=\frac{\Delta\gamma_{max}}{2}+0.5\Delta\varepsilon_n+\frac{\sigma_{n,max}}{\sigma_y}\frac{\Delta\varepsilon_n}{2}$ $=A\frac{\sigma_f'}{E}(2N_f)^b+B\varepsilon_f'(2N_f)^c+C\frac{\sigma_f'^2}{E\sigma_y}(2N_f)^{2b}+D\frac{\sigma_f'\varepsilon_f'}{\sigma_y}(2N_f)^{b+c}$	[6]
	IG	$\frac{\Delta\varepsilon_{gen}^*}{2}=\left(\frac{\tau_{max}}{\tau_f'}\frac{\Delta\gamma^e}{2}+\frac{\Delta\gamma^p}{2}+\frac{\sigma_{n,max}}{\sigma_f'}\frac{\Delta\varepsilon_n^e}{2}+\frac{\Delta\varepsilon_n^p}{2}\right)_{max}$ $=\frac{\sigma_f'}{E}(2N_f)^b+\varepsilon_f'(2N_f)^c$	[7,8]
	ZWW	$\varepsilon_{eq}=k(1+\alpha\Phi_{ZWW})\varepsilon_{\pi,max}=\frac{\sigma_f'}{E}(2N_f)^b+\varepsilon_f'(2N_f)^c$	[9,10]
Stress/Strain	FS	$\frac{\Delta\gamma}{2}\left(1+\kappa_{FS}\frac{\sigma_{n,max}}{\sigma_y}\right)=\frac{\tau_f'}{G}(2N_f)^{b'}+\gamma_f'(2N_f)^{c'}$	[11]
Energy	SWT	$\frac{\Delta\varepsilon}{2}\sigma_{n,max}=\frac{\sigma_f'^2}{E}(2N_f)^{2b}+\sigma_f'\varepsilon_f'(2N_f)^{2c}$	[1,12,13]
	Ellyin	$(\Delta w^p/\bar{\rho})+\Delta w^{e+}=k(N_f)^\alpha+C$	[14]
	Liu I	$(\Delta\sigma_n\Delta\varepsilon_n)_{max}+(\Delta\tau\Delta\gamma)=\frac{4\sigma_f'^2}{E}(2N_f)^{2b}+4\sigma_f'\varepsilon_f'(2N_f)^{b+c}$	[15]
	Liu II	$(\Delta\sigma_n\Delta\varepsilon_n)+(\Delta\tau\Delta\gamma)_{max}=\frac{4\tau_f'^2}{G}(2N_f)^{2b'}+4\tau_f'\gamma_f'(2N_f)^{b'+c'}$	[15]
	CCB	$\left(\sigma_{n,max}\frac{\Delta\varepsilon_n}{2}+\tau_{max}\frac{\Delta\gamma_n}{2}\right)_{max}=\frac{4\tau_f'^2}{G}(2N_f)^{2b'}+4\tau_f'\gamma_f'(2N_f)^{b'+c'}$	[16]
	Chen	$\Delta\gamma_{max}\Delta\tau+\Delta\varepsilon_n\Delta\sigma_n=\frac{4\tau_f'^2}{G}(2N_f)^{2b'}+4\tau_f'\gamma_f'(2N_f)^{b'+c'}$	[17]
(Part II)			
Energy	MSWT	$DP_{MSWT}=2a\Delta\varepsilon\langle\sigma_{max}\rangle+\frac{1-a}{2}\Delta\gamma\Delta\tau$ $=\frac{4a\sigma_f'^2}{E}(2N_f)^{2b}+4\sigma_f'\varepsilon_f'(2N_f)^{b+c}$	[18–20]
	Varvani	$W_{VF}=\frac{\Delta\sigma_n\Delta\varepsilon_n}{\sigma_f'\varepsilon_f'}+\frac{\Delta\tau_{max}\Delta\gamma_{max}}{2\tau_f'\gamma_f'}$ $=\left[\frac{\sigma_f'}{E}(2N_f)^b+\varepsilon_f'(2N_f)^c\right]+\left[\frac{\tau_f'}{G}(2N_f)^{b'}+\gamma_f'(2N_f)^{c'}\right]$	[21–23]
	Lazzarin	$\Delta W_t=\frac{1}{2}[(K_{t,b}\cdot\Delta\sigma_{nom})^2+2(1+\nu)(K_{t,t}\cdot\Delta\tau_{nom})^2]=f(N_f)$	[24–26]
	Lagoda	$\frac{\sigma_{axx}^2}{\tau_{axy}^2(1+\nu_e)}W_{a\eta s}+\frac{4}{1-\nu_e}\left(1-\frac{\sigma_{axx}^2}{\tau_{axy}^2}\right)W_{a\eta}=\frac{\sigma_f'^2}{2E}(2N_f)^{2b}$	[27–30]
	Zhu	$\left(\frac{\sigma_{max}^2}{2E}\right)+\zeta\left(\frac{\tau_{max}^2}{2G}\right)+\left(\Delta\sigma\Delta\varepsilon_p\frac{1-h_c}{1+h_c}\right)+\zeta\left(\Delta\tau\Delta\gamma_p\frac{1-h_c}{1+h_c}\right)$ $=\left(\frac{\sigma_c^2(2N_f)^{2b}}{2E}\right)+\zeta\left(\frac{\tau_c^2(2N_f)^{2b'}}{2G}\right)$ $+4\frac{c-b}{c+b}\left[\sigma_c\varepsilon_c(2N_f)^{b+c}+\zeta\tau_c\gamma_c(2N_f)^{b'+c'}\right]$	[31]
	Branco	$\Delta W_T=\Delta W_e^+\zeta\Delta W_p=\kappa_T(2N_f)^{\alpha_T}+\Delta W_0$ $\Delta W_e^+=\left[\frac{1+\nu}{3E}(\sigma_{eq}^{max})^2+\frac{1-2\nu}{6E}\left(\sum_{i=1}^{3}(\sigma_i^a+\sigma_i^m)\right)^2\right]$ $\Delta W_p=\left[\frac{2(1-n')}{1+n'}(2K')^{-\frac{1}{n'}}(\Delta\sigma_{eq})^{\frac{1+n'}{n'}}\right]$	[32–34]
	Lu	$FP=(1-a)E_{N1max}-aE_{N1min}+b[(1-a)E_{N2max}-aE_{N2min}]$ $+c(E_{S1max}-E_{S1min}+E_{S2max}-E_{S2min})$ $=A(2N_f)^B+C(2N_f)^D$	[35,36]
	SNSER	$\hat{M}_{eq}=(1+\kappa\Phi_{YS})[\alpha\Delta\sigma\Delta\varepsilon+(1-\alpha)\Delta\tau\Delta\gamma]_{max}$ $=\frac{4\sigma_f'^2}{E}(2N_f)^{2b}+4\sigma_f'\varepsilon_f'(2N_f)^{b+c}$ or $=\frac{6}{1+\nu_e}\frac{\tau_f'^2}{G}(2N_f)^{2b'}+4\tau_f'\gamma_f'(2N_f)^{b'+c'}$	This paper

component ($\sqrt{3}\tau$ vs. σ) with regard to the complex loading path in strain controlling mode.

Responding to mentioned challenges, that is the applicability and feasibility of multiaxial fatigue criteria on performing the service safety of engineering components. In this study, a novel energy-based multiaxial fatigue life prediction model was developed considering the effects of both the normal strain energy and shear strain energy on the failure of materials. Additionally, the new proposed criterion considered the difference of contributions of both the normal strain energy and

shear strain energy on the failure of materials. Meanwhile, the energy weight coefficient α was introduced, which is a stress-path-dependent parameter acquired from the stable hysteresis loops. Moreover, the new proposed criterion considered the effect of non-proportionality on multiaxial fatigue performance of SS304, which was also defined as a stress-path-dependent parameter. Notably, most of the parameters in the new criterion can be determined by monotonic tensile mechanical properties (including the uniaxial/torsional fatigue parameters and the non-proportional cyclic hardening factor), which improved the engineering applicability and feasibility of the criterion. Finally, this paper presents the performance of the new criterion from the others by comparing the predicted fatigue life with the tested results, which highlighted the satisfactory performance of the new one.

2. New multiaxial fatigue criterion considering the shear/normal strain energy ratio

2.1. Definition of the damage parameter

For the issue of multiaxial fatigue of metal materials, the combination of various stress components and the varying principal stress direction, as well as the complex failure mechanism (tensile (or normal) dominated failure or shear dominated failure caused by the difference of microstructure thereby the mechanical properties of the material work together and complicate the multiaxial fatigue life prediction [41]. The most commonly used choice to deal with the multiaxial fatigue problem of metal materials is the critical plane method [4]: in the face of the complex loading process, finding the maximum damage indicator according to the material failure criterion is obviously a more wise choice than considering the contribution of all stress–strain components in an all-round way, because it greatly simplifies the problem by considering the material failure mechanism.

In the process of uniaxial or multiaxial fatigue life prediction, this study attempts to use a more balanced model to describe the failure of materials, even if the failure mechanism of different metal materials varies. In other words, due to the effect of material microstructure, the material is characterized by tensile dominated failure or shear dominated failure. Typically, cast iron is characterized by tensile dominant failure while low carbon steel is characterized by shear dominant failure, which illustrates that the tensile dominant models with normal stress/strain components such as SWT model ($\Delta\varepsilon\sigma_{n,max}/2$) and Liu I model ($(\Delta\sigma_n\Delta\varepsilon_n)_{max}+(\Delta\tau\Delta\gamma)$) are used for strong brittle materials to obtain better multiaxial fatigue life prediction results, while the shear dominant models such as Liu II model ($(\Delta\sigma_n\Delta\varepsilon_n)+(\Delta\tau\Delta\gamma)_{max}$) and Chen's model ($\Delta\gamma_{max}\Delta\tau+\Delta\varepsilon_n\Delta\sigma_n$) are used for strong ductile materials to obtain better multiaxial fatigue life prediction results.

However, the ductility and brittleness of metal materials are not so extreme, that is, both the normal components and the shear components contribute to the failure of materials, but the sensitivity of materials to the normal and shear components is different. At the same time, in the sense of physical mechanics, whether in the form of normal or shear, or even their combination to define the failure of materials, it is necessary to meet the principle that the energy driving the failure of materials is constant. On the critical plane, following the views of Liu [15], CCB [16], Chen [17], MSWT [12,19,20], Varvani [21–23], Lazzarin [24–26], Zhu [31], Lagoda [27–30] and Lu [35,36], it is reasonable to believe that the multiaxial failure of metal materials is the cooperative contribution of the normal and shear components. Therefore, on the critical plane, the total strain energy ($\hat{M}$) driving material to failure consists of two parts, namely normal strain energy component ($\hat{E}$) and shear strain energy component($\hat{G}$), and $\hat{M}=\hat{E}+\hat{G}$. However, the view that the failure of materials is the contribution of the same weight of tensile strain energy and shear strain energy is fairly extreme. Therefore, it is suggested to introduce the energy weight coefficient (α) to coordinate the contribution weight of normal strain energy and shear strain energy in material failure, which is affected by the elastoplastic response of the material during multiaxial loading. In other words, even under the same loading command (strain controlled loading), different materials will show various mechanical behaviors (stress response), which is the intention of this study to determine the energy weight coefficient by using the stress path (Fig. 2). Thus, Failure of structures is the result of irreversible energy accumulation in hotspots. The total strain energy ($\hat{M}$) against normal strain energy component ($\hat{E}$) and shear strain energy component($\hat{G}$) is given by

$$\hat{M}=\alpha\hat{E}+(1-\alpha)\hat{G}, \tag{1}$$

where α is the energy weight coefficient and $\alpha\in[0,1]$. Apparently, α plays the role of weight coordination, taking α value between 0 and 1, so as to ensure the constancy of total strain energy.

Once the material and service temperature are specified, the monotonic/cyclic mechanical properties of the material are obtained. In regard to the critical plane method, whether it is the normal strain energy criterion, the shear strain energy criterion, and the linear combination of normal strain energy and shear strain energy as Eq. (1), the energy driving the material to failure is the intrinsic parameter. Accordingly, it is reasonable to believe that the energy driving material to failure under the most extreme conditions, such as pure shear condition ($\alpha=0$) and pure tensile condition ($\alpha=1$), is equal. Therefore, gives

$$\hat{E}=\hat{G}. \tag{2}$$

Continuing the studies of Liu [15], CCB [16], Chen [17], MSWT [12,19,20], Varvani [21–23], Zhu [31] and Lu [35,36], on the critical plane, the normal strain energy and shear strain energy are expressed by the product of the stress and strain variation range in the loading process, namely $\Delta\sigma\Delta\varepsilon$ and $\Delta\tau\Delta\gamma$. Combining Eqs. (1) and (2), the total strain energy can be further expressed as

$$\hat{M}=\alpha\Delta\sigma\Delta\varepsilon+(1-\alpha)\Delta\tau\Delta\gamma, \tag{3}$$

Since the introduction of critical plane degenerates the varying principal stress plane during multiaxial fatigue loading to a stable plane, Liu, CCB, Chen and MSWT criteria establish the relationship between strain energies and fatigue life (N_f) through fatigue parameters (σ_f' or τ_f', ε_f' or γ_f', b or b', c or c'). Accordingly, the relationship between total strain energy and fatigue life is suggested as

$$\hat{E}=\Delta\sigma\Delta\varepsilon=\frac{4\sigma_f'^2}{E}(2N_f)^{2b}+4\sigma_f'\varepsilon_f'(2N_f)^{b+c}. \tag{4}$$

Considering that the relationship between shear strain energy and fatigue life has the same form as the above formula, gives

$$\hat{G}=\Delta\tau\Delta\gamma=m_1\frac{\tau_f'^2}{G}(2N_f)^{2b'}+m_2\tau_f'\gamma_f'(2N_f)^{b'+c'}. \tag{5}$$

Above $\Delta\sigma$ and $\Delta\tau$ are normal/shear stress ranges in a loading cycle. $\Delta\varepsilon$ and $\Delta\gamma$ are normal/shear strain ranges in this loading cycle. σ_f', ε_f', b and c as well as τ_f', γ_f', b' and c' are fatigue parameters in normal and shear forms respectively, namely fatigue strength coefficient, fatigue ductility coefficient, fatigue strength exponent and fatigue ductility exponent as well as shear fatigue strength coefficient, shear fatigue ductility coefficient, shear fatigue strength exponent and shear fatigue ductility exponent. E and G are Young's modulus and shear modulus. m_1 and m_2 are undetermined coefficients.

Since the strain energy components on the left of Eqs. (4) and (5) indicate the intrinsic properties driven to material failure. Therefore, whether expressed in normal strain energy (Eq. (5)) or shear strain energy (Eq. (5)), the equivalence of the criteria should be satisfied. This requires that the expressions expressed in the form of fatigue life and fatigue parameters on the right of Eqs. (4) and (5) are also equal. Therefore, m_1 and m_2 are introduced. Substituting Eqs. (4) and (5) into Eq. (2) yields

$$\frac{4\sigma_f'^2}{E}(2N_f)^{2b}+4\sigma_f'\varepsilon_f'(2N_f)^{b+c}=m_1\frac{\tau_f'^2}{G}(2N_f)^{2b'}+m_2\tau_f'\gamma_f'(2N_f)^{b'+c'}. \tag{6}$$

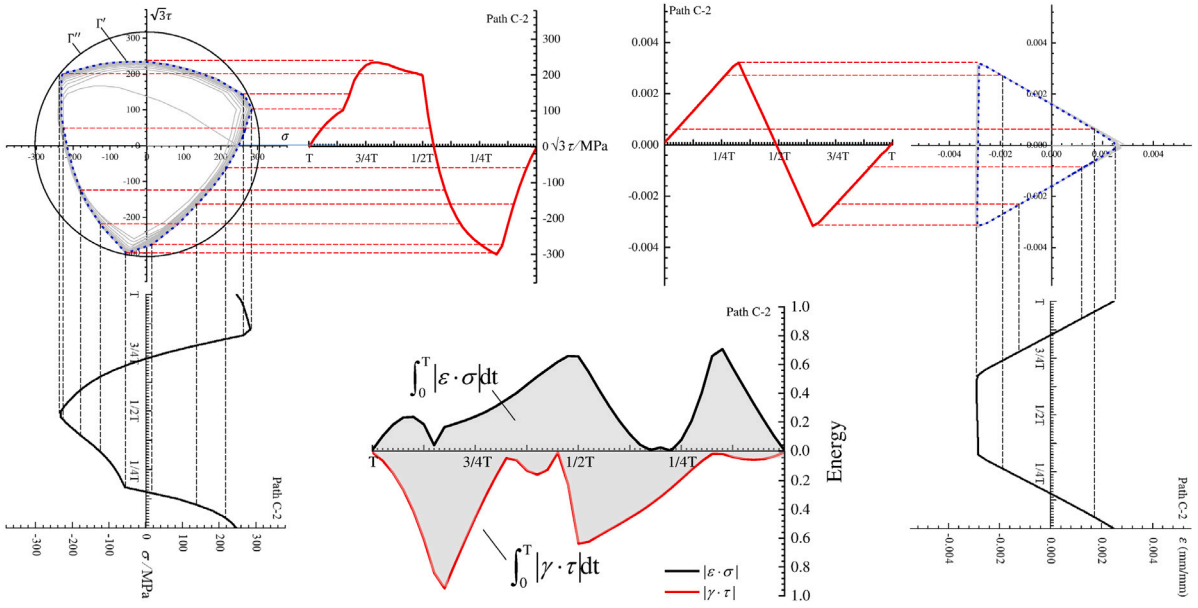

Fig. 2. Definition of loading path based on the stress responding as well as the corresponding energy evolution in a loading cycle under the condition of cyclic stability. (For interpretation of the references to color in this figure legend, the reader is referred to the web version of this article.)

or

$$\begin{cases} \dfrac{4\sigma_f'^2}{E}(2N_f)^{2b} = m_1 \dfrac{\tau_f'^2}{G}(2N_f)^{2b'}, \\ 4\sigma_f'\varepsilon_f'(2N_f)^{b+c} = m_2\tau_f'\gamma_f'(2N_f)^{b'+c'}. \end{cases} \tag{7}$$

Since the relationship between Young's modulus and the shear modulus can be expressed as

$$G = \frac{E}{2(1+\nu_e)}, \tag{8}$$

and the relationship between normal and shear fatigue parameters satisfy [41–43]

$$\begin{cases} \tau_f' = \dfrac{\sigma_f'}{\sqrt{3}}, \quad \gamma_f' = \sqrt{3}\varepsilon_f', \\ b' = b, \quad c' = c. \end{cases} \tag{9}$$

Substituting Eqs. (8) and (9) into Eq. (7) yields

$$m_1 = \frac{6}{1+\nu_e}, \quad m_2 = 4. \tag{10}$$

Introducing Eq. (10) into Eqs. (4) and (5) yields

$$\begin{cases} \hat{E} = \dfrac{4\sigma_f'^2}{E}(2N_f)^{2b} + 4\sigma_f'\varepsilon_f'(2N_f)^{b+c}, \\ \hat{G} = \dfrac{6}{1+\nu_e}\dfrac{\tau_f'^2}{G}(2N_f)^{2b'} + 4\tau_f'\gamma_f'(2N_f)^{b'+c'}. \end{cases} \tag{11}$$

Correlating Eq. (11) with Eq. (3) yields

$$\begin{cases} \alpha\hat{E} = \alpha\Delta\sigma\Delta\varepsilon = \alpha\left[\dfrac{4\sigma_f'^2}{E}(2N_f)^{2b} + 4\sigma_f'\varepsilon_f'(2N_f)^{b+c}\right], \\ (1-\alpha)\hat{G} = (1-\alpha)\Delta\tau\Delta\gamma \\ = (1-\alpha)\left[\dfrac{6}{1+\nu_e}\dfrac{\tau_f'^2}{G}(2N_f)^{2b'} + 4\tau_f'\gamma_f'(2N_f)^{b'+c'}\right]. \end{cases} \tag{12}$$

In accordance with the definition of total strain energy in Eq. (1), it is, therefore eventual to obtain

$$\begin{aligned} \hat{M} &= \alpha\hat{E} + (1-\alpha)\hat{G} \\ &= \alpha\left[\frac{4\sigma_f'^2}{E}(2N_f)^{2b} + 4\sigma_f'\varepsilon_f'(2N_f)^{b+c}\right] \\ &+ (1-\alpha)\left[\frac{6}{1+\nu_e}\frac{\tau_f'^2}{G}(2N_f)^{2b'} + 4\tau_f'\gamma_f'(2N_f)^{b'+c'}\right]. \end{aligned} \tag{13}$$

Correlating with Eq. (8), Eq. (13) can be further simplified into

$$\begin{aligned} &\hat{M} = \alpha\hat{E} + (1-\alpha)\hat{G} = \frac{4\sigma_f'^2}{E}(2N_f)^{2b} + 4\sigma_f'\varepsilon_f'(2N_f)^{b+c}, \\ &\text{or} = \frac{6}{1+\nu_e}\frac{\tau_f'^2}{G}(2N_f)^{2b'} + 4\tau_f'\gamma_f'(2N_f)^{b'+c'}. \end{aligned} \tag{14}$$

For pure tension/compression loading conditions, $\alpha = 1$ and for pure torsion loading conditions, $\alpha = 0$, then Eq. (14) can be simplified into

$$\begin{cases} \hat{E} = \dfrac{4\sigma_f'^2}{E}(2N_f)^{2b} + 4\sigma_f'\varepsilon_f'(2N_f)^{b+c}, \\ \hat{G} = \dfrac{6}{1+\nu_e}\dfrac{\tau_f'^2}{G}(2N_f)^{2b'} + 4\tau_f'\gamma_f'(2N_f)^{b'+c'}. \end{cases} \tag{15}$$

Eq. (15) is the same as Eq. (11), which is the model in both normal and shear form.

2.2. Correlation between the energy weight coefficient and the torsion–tension energy ratio

In practical analysis, multiaxial fatigue life prediction were conducted when reasonably the cyclic response is stable. It is, usually, donated the half-failure life as the stable cycle. Therefore, in this paper, the stress/strain responses in the stable cycles were extracted to characterize the shear strain energy and normal strain energy responses of different loading paths. Fig. 2 shows the strain-controlled loading path, namely C-2 tested in this paper, along with the corresponding stress components. Both of the stress and strain paths were highlighted by blue-dash line. Accordingly, the cumulative normal strain energy and shear strain energy in the stable cycles in terms of the shaded areas were identified, respectively. Furthermore, the need for a reasonable

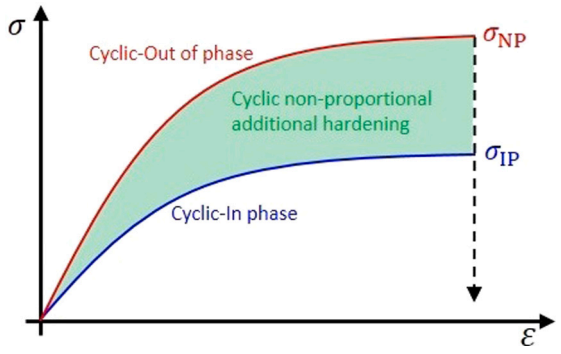

Fig. 3. Schematic illustration of the non-proportional induced cyclic hardening for metallic materials.

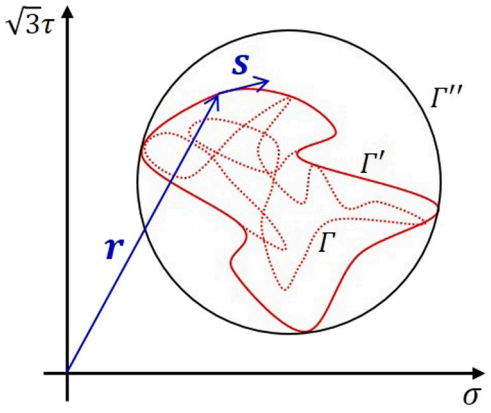

Fig. 4. Normal stress versus shear stress during the loading process.

clarification of the different contribution of normal strain energy and shear strain energy on fatigue failure, considering cyclic, non-linear response of the material to multiaxial loading, is addressed, together with the definition of the torsion–tension energy ratio. Here gives the expression of torsion–tension energy ratio ξ as

$$\xi = \frac{(1-\alpha)\hat{G}}{\alpha\hat{E}} = \frac{1-\alpha}{\alpha} = \frac{\int_0^T |\frac{\gamma}{\sqrt{3}} \cdot \sqrt{3}\tau| \mathrm{d}t}{\int_0^T |\varepsilon \cdot \sigma| \mathrm{d}t} = \frac{\int_0^T |\gamma \cdot \tau| \mathrm{d}t}{\int_0^T |\varepsilon \cdot \sigma| \mathrm{d}t}, \tag{16}$$

or

$$\alpha = \frac{1}{1+\xi} = \frac{\int_0^T |\varepsilon \cdot \sigma| \mathrm{d}t}{\int_0^T |\varepsilon \cdot \sigma| \mathrm{d}t + \int_0^T |\gamma \cdot \tau| \mathrm{d}t}. \tag{17}$$

2.3. Non-proportionality effects

The complex multiaxial loading behavior will introduce non-proportional additional hardening, which may significantly affect the fatigue life prediction. Fig. 3 schematically illustrates the non-proportional induced cyclic hardening for metallic materials. Therefore, the non-proportionality, Φ is introduced to take into account the effect of non-proportional additional hardening. A commonly used form [44] relates multiaxial damage parameters to non-proportional additional hardening, which has been successfully applied in many researches [9,10,45]. Therefore, the equivalent damage parameter $\hat{M}_{\mathrm{eq}}$ suggested in this paper can be expressed as

$$\hat{M}_{\mathrm{eq}} = (1 + \kappa\Phi_{\mathrm{YS}})\hat{M}, \tag{18}$$

where κ is the non-proportional cyclic hardening factor, which represents the sensitivity of the material to non-proportional loading, and therefore the microstructure of the material. Therefore, Itoh et al. [46,47] introduced an expression of the non-proportional additional hardening factor κ for FCC (face-centered cubic structure) and BCC (body-centered cubic structure) respectively

$$\begin{cases} \kappa = \dfrac{\sigma_{\mathrm{b}} - \sigma_{\mathrm{y}}}{\sigma_{\mathrm{b}}} & \text{for FCC material,} \\ \kappa = 2\dfrac{\sigma_{\mathrm{b}} - \sigma_{\mathrm{y}}}{\sigma_{\mathrm{b}}} & \text{for BCC material,} \end{cases} \tag{19}$$

where σ_{b} is the ultimate stress and σ_{y} is the yield stress.

Fig. 4 shows the stress–strain curve of random multiaxial loading path, where Γ and Γ' represent the complete path of the loading cycle, Γ and Γ' are the outermost and inner curves of the complete loading path respectively. Γ'' represents the minimum circumscribed contour of the path. Therefore, in consideration of the loading path, the above approach simplifies the effect of non-proportional loading reasonably and effectively.

Investigations on the non-proportionality, Φ have been widely carried out. Socie [1] developed a simple definition on the non-proportionality, which introduced an ellipse with a minimum area to enclose the whole loading path and the ratio of the minor axis b_{ax} to major axis a_{ax} can be calculated as the non-proportionality.

$$\Phi_{\mathrm{Socie}} = \frac{b_{ax}}{a_{ax}}, \tag{20}$$

Socie's definition is simple and practical, but it does not consider the influence of the loading path, which leads to poor accuracy in predicting the life of a complex loading path. Chen [48] related the geometry of the strain loading path with the hardening mechanism and defined the non-proportionality as

$$\Phi_{\mathrm{Chen}} = 2\frac{A_{\Gamma'}}{A_{\Gamma''}} - 1, \tag{21}$$

Borodii et al. [49] considered the non-proportionality parameter Φ as

$$\Phi_{\mathrm{Borodii}} = \left(\frac{|\oint_{\Gamma'} \mathbf{e} \times \mathrm{d}\mathbf{e}|}{|\oint_{\Gamma''} \mathbf{e} \times \mathrm{d}\mathbf{e}|} \right)^r, \tag{22}$$

where $\mathbf{e}$ and $\mathrm{d}\mathbf{e}$ are the vectors of strain and strain increment, respectively. Γ' and Γ'' indicate the deformation paths defined similar to Fig. 4. Based on Meggiolaro and Castro's research [50], in which moment of inertia was introduced to characterize the arbitrary loading path and the MOI (Moment Of Inertia) method was developed, Zhong et al. [9] further optimized the MOI method and proposed the expression form of non-proportionality as follows

$$\Phi_{\mathrm{ZWW}} = \left(\frac{I_{\Gamma'}}{I_{\Gamma''}} \right)^s, \tag{23}$$

where $I_{\Gamma'}$ and $I_{\Gamma''}$ are the moment of inertia of x-axis of the equivalent convex strain (or stress) loading path Γ' and Γ'' as illustrated in Fig. 4. Moreover, Araújo [51], Paul [52] and Zhu [53] gave the definition of non-proportionality from different views. However, in multiaxial fatigue test, strain-controlled mode is often used, and the elastoplastic behavior of materials cannot be fully characterized only by strain loading path as the definition of non-proportionality. Therefore, in this paper, the non-proportionality, Φ based on stress loading path was defined

$$\Phi_{\mathrm{YS}} = \frac{|\oint_{\Gamma'} \mathbf{r} \times \mathrm{d}\mathbf{s}|}{|\oint_{\Gamma''} \mathbf{r} \times \mathrm{d}\mathbf{s}|}, \tag{24}$$

where $\mathbf{r}$ and $\mathrm{d}\mathbf{s}$ are the vectors of stress and stress increment, respectively. Γ' and Γ'' indicate the stress paths defined in Fig. 4. The concept of definition on non-proportionality in this paper is similar to that of Borodii [49], the difference is that this paper defined the non-proportionality based on stress path. Therefore, it is not necessary to introduce non-linear parameters like Borodii (exponent parameter, r in Eq. (22)), which obviously simplifies the difficulty of quantifying non-proportionality.

3. Cyclic plasticity modeling on the SS304

Since the deformation behavior of SS304 is complex with regard to the over complicated mechanical properties as well as the proportional and non-proportional loading spectrum. It is necessary to introduce a reliable cyclic plasticity model to modeling the stress/strain process of specimens under multiaxial loading conditions so as to further predict the fatigue life.

3.1. The constitutive model

Cyclic plasticity behavior of homogeneous materials under cyclic loadings has troubled scholars for decades during which various models were proposed. In this study, the Ohno–Wang [54] nonlinear kinematic model is introduced which successfully described closed stress–strain hysteresis loops for the strain rate independent material and predicted ratcheting behavior. Based on the theory of elastoplastic in material deformation, the main equations are

$$\varepsilon_{ij} = \varepsilon_{ij}^{\mathrm{e}} + \varepsilon_{ij}^{\mathrm{p}}, \tag{25}$$

$$\sigma_{ij} = C_{ijkl} : \varepsilon_{ij}^{\mathrm{p}}, \tag{26}$$

and

$$\dot{\varepsilon}_{ij}^{\mathrm{e}} = \dot{\lambda}\frac{\partial f}{\partial \sigma_{ij}}. \tag{27}$$

where ε_{ij} is the total strain tensor which is decomposed into the elastic strain tensor $\varepsilon_{ij}^{\mathrm{e}}$ and the plastic strain tensor $\varepsilon_{ij}^{\mathrm{p}}$. The stress tensor σ_{ij} and elastic strain $\varepsilon_{ij}^{\mathrm{e}}$ subjected to Hooke's law with the elastic stiffness tensor. The flow rule gives the relationship between the plastic strain rate $\dot{\varepsilon}^{\mathrm{p}}$ and stress increment, in which $\dot{\lambda}$ is an undetermined scalar multiplier and F is the plastic potential function, as

$$F = \sqrt{\frac{3}{2}\left(s_{ij} - \alpha_{ij}\right) : \left(s_{ij} - \alpha_{ij}\right)} - Y. \tag{28}$$

Where s_{ij} is the deviatoric part of stress tensor, α_{ij} is the deviatoric part of back stress tensor, Y is the size of yield surface. For the Von Mises yield criterion, we can use the expression for effective plastic strain rate in Eq. (27) to write a similar expression for the increment in effective plastic strain as

$$\dot{p} = \sqrt{\frac{2}{3}\dot{\varepsilon}_{ij}^{p} : \dot{\varepsilon}_{ij}^{p}}. \tag{29}$$

3.2. Kinematic hardening

With regard to the cyclic deformation induced translation and expansion of yield surface, Chaboche et al. [55] argued the back stress α_{ij} can be divided into m components, as

$$\alpha_{ij} = \sum_{k=1}^{m} \alpha_{ij}^{k}. \tag{30}$$

For each back stress component α_{ij}^{k}, Ohno and Wang suggested

$$f^{k} = (\bar{\alpha}^{k})^{2} - (r^{k})^{2} \tag{31}$$

as the critical state in the dynamic recovery term [54]. Following the discussion of Döring [56], Abdel-Karim [57] and Kang [58], Fang [59] suggested the description of back stress as

$$\dot{\alpha}_{ij}^{k} = h^{k}\frac{2}{3}\dot{\varepsilon}_{ij}^{p} - H(f^{k})\dot{\omega}^{k}\frac{\alpha_{ij}^{k}}{r^{k}}. \tag{32}$$

which was also verified by Sun and Yuan [60].

Above $\bar{\alpha}^{k} = \sqrt{\frac{2}{3}\alpha_{ij}^{p} : \alpha_{ij}^{p}}$. Both h^{k} and r^{k} denote the state variables. f^{k} represents the critical state surface in the deviatoric stress space. $H(\cdot)$ is the Heaviside step function. $\dot{\omega}^{k}$ can be further expressed by supposing $\dot{f}^{k} = 0$ [54], that is

$$\begin{aligned} \dot{f}^{k} &= 3\alpha_{ij}^{k}\dot{\alpha}_{ij}^{k} - 2r^{k}\dot{k}^{k} \\ &= 3\alpha_{ij}^{k}\left[h^{k}\frac{2}{3}\dot{\varepsilon}_{ij}^{p} - H(f^{k})\dot{\omega}^{k}\frac{\alpha_{ij}^{k}}{r^{k}}\right] - 2r^{k}\dot{k}^{k} = 0. \end{aligned} \tag{33}$$

When $H(f^{k}) = 1$, $\dot{\omega}^{k}$ can be finally expressed as

$$\dot{\omega}^{k} = h^{k}\frac{\alpha_{ij}^{k}}{r^{k}} : \dot{\varepsilon}_{ij}^{p} - \dot{r}^{k}. \tag{34}$$

Substituting Eq. (34) into Eq. (32) and then combining with the Armstrong and Frederick model developed by Adbel-Karim and Ohno [57], the kinematic hardening rule is given by

$$\begin{aligned} \dot{\alpha}_{ij}^{k} = {} & r^{k}\zeta^{k}\left[\frac{2}{3}\dot{\varepsilon}_{ij}^{p} - \mu^{k}\frac{\alpha_{ij}^{k}}{r^{k}}\dot{p}\right. \\ & \left. - H(f^{k})\left\langle\frac{\alpha_{ij}^{k}}{r^{k}} : \dot{\varepsilon}_{ij}^{p} - \mu^{k}\dot{p}\right\rangle\frac{\alpha_{ij}^{k}}{r^{k}}\right] + H(f^{k})\frac{\alpha_{ij}^{k}}{r^{k}}\dot{r}^{k}. \end{aligned} \tag{35}$$

Above k represents the number of the individual back stress α_{ij}^{k}, and α_{ij} is the summation of back stress. ζ^{k} is material constant satisfying $h^{k} = r^{k}\zeta^{k}$. μ^{k} ($\in (0,1)$) is introduced to describe the ratcheting and cyclic stress relaxation behavior. Meanwhile, Eq. (35) can be reasonably reduce to the known Ohno and Wang model and the Armstrong and Frederick model by giving $\dot{r}^{k} = 0 \& \mu^{k} = 0$ and $\dot{r}^{k} = 0 \& \mu^{k} = 1$ respectively.

3.3. Cyclic hardening

The fatigue tests of SS304 show that the cyclic hardening takes numerous cycles to saturate, resulting stabilized mechanical performance. Following Ohno and Wang's work, Fang suggested to describe uniaxial isotropic hardening by changing r^{k}, which can be reasonably divided into two components [59], that is

$$r^{k} = r_{0}^{k} + r_{\Delta}^{k} \tag{36}$$

with r_{0}^{k} and r_{Δ}^{k} can be respectively estimated from the monotonic and stabilized hysteresis loop. As described in [60], the cyclic mechanical behavior of the elastoplastic material r_{Δ}^{k} is assumed to depend on the accumulated plastic strain, $p = \left(\frac{2}{3}\varepsilon_{ij}^{\mathrm{p}} : \varepsilon_{ij}^{\mathrm{p}}\right)^{1/2}$, as

$$r_{\Delta}^{k} = r_{\Delta s}^{k}[1 - a_{1}^{k}e^{-b_{1}^{k}p} - (1 - a_{1}^{k})e^{-b_{2}^{k}p}]. \tag{37}$$

Chaboche proposed the plastic strain based memory surface, as

$$g = \sqrt{\frac{2}{3}\left(\varepsilon_{ij}^{p} - \beta_{ij}\right) : \left(\varepsilon_{ij}^{p} - \beta_{ij}\right)} - q. \tag{38}$$

Above β_{ij} and q denote the radius and center of the non-hardening surface. The update of memory state can only be activated in a specific plastic strain state, that is the current plastic strain is on the surface ($g = 0$) and the flow direction is outward from the surface ($(\partial g/\partial \varepsilon_{ij}^{p}) : \mathrm{d}\varepsilon_{ij}^{p} \geq 0$). The evolution of β and q follows

$$\begin{cases} \dot{\beta} = (1-\eta)H(g)\langle n_{ij} : n_{ij}^{*}\rangle\sqrt{\frac{3}{2}}n_{ij}^{*}\dot{p} \\ \dot{q} = \eta H(g)\langle n_{ij} : n_{ij}^{*}\rangle\dot{p} \end{cases} \tag{39}$$

with $n_{ij} = \partial F/\partial \sigma_{ij}$ and $n_{ij}^{*} = \partial g/\partial \sigma_{ij}^{p}$.

3.4. Non-proportional hardening

As illustrated in Fig. 3, additional hardening phenomenon is identified with regard to the cyclic non-proportional loads termed of non-proportional hardening, which can be described by the dynamic evolution of yield surface Y, as

$$Y = Y_{0} + Y_{\Delta \mathrm{np}}. \tag{40}$$

Table 2
Elastoplastic parameters of SS304.

E = 198 GPa, ν_e = 0.3, σ_0 = 160 MPa									
k	1	2	3	4	5	6	7	8	9
ζ^k	20 000.0	10 000.0	5000.0	2000.0	1000.0	500.0	200.0	100.0	50.0
r_0^k	16.04	38.46	35.78	28.82	8.95	10.86	5.99	18.63	1.0
$r_{\Delta s}^k$	−2.35	−28.12	−17.58	5.79	30.32	25.70	26.34	33.84	1.0
a_1^k=1, b_1^k=120, b_2^k=2, k = 1, 2...9									
μ=0.2, γ_p=10, γ_q=97, $Y_{\Delta\text{sat}}$=100, c_c=50									

Above Y_0 is the yield stress corresponding to proportional loading, $Y_{\Delta\text{np}}$ is defined by

$$\dot{Y}_{\Delta\text{np}} = \gamma_\text{p}\left(Y_{\Delta\text{nps}} - Y_{\Delta\text{np}}\right)\dot{p}, \tag{41}$$

representing the non-proportional hardening.

Integrating Eq. (41) with initial condition $Y_{\Delta\text{np}}(0) = 0$, yields

$$Y_{\Delta\text{np}} = Y_{\Delta\text{nps}}\left(1 - e^{-\gamma_\text{p} p}\right), \tag{42}$$

where $Y_{\Delta\text{nps}}$ denotes the saturated value of $Y_{\Delta\text{np}}$ under a specified non-proportional loading path. During the calculation process, the non-proportionality Φ was introduced by Tanaka and expressed as [61]

$$\Phi_{\text{Tanaka}} = \sqrt{1 - \frac{n_{\alpha\beta}C_{\zeta\zeta\alpha\beta}C_{\zeta\zeta\gamma\eta}n_{\gamma\eta}}{C_{ijkl}C_{ijkl}}}, \tag{43}$$

where C_{ijkl} is the fourth-rank tensor and denotes the internal dislocation structure, as [61]

$$\dot{C}_{ijkl} = c_c\left(n_{ij}\otimes n_{kl} - C_{ijkl}\right)\dot{p}. \tag{44}$$

Sun assumed that $Y_{\Delta\text{nps}}$ follows [60]

$$Y_{\Delta\text{nps}} = \Phi_{\text{Tanaka}} Y_{\Delta\text{NS}}, \tag{45}$$

where Φ_{Tanaka} ranges from 0 to 1, corresponding to the loading state vary from no non-proportional hardening to the maximum non-proportional hardening. Accordingly, the evolution of $Y_{\Delta\text{NS}}$ was suggested to be defined as

$$\dot{Y}_{\Delta\text{NS}} = \gamma_\text{q}\left(Y_{\Delta\text{sat}} - Y_{\Delta\text{NS}}\right)\dot{q}, \tag{46}$$

where q denotes the radius of strain memory surface. The rate parameter γ_q is reduced to 0 considering the Masing postulate. Accordingly, $Y_{\Delta\text{sat}}$ represents the saturate value of $Y_{\Delta\text{NS}}$.

3.5. Determination of the elastic–plastic parameters of SS304 and implementations of the cyclic plasticity in FEM

The monotonic and cyclic mechanical properties of SS304 will be illustrated below and available in Table 4. Further more, [62] and [63] suggested

$$\zeta^k = \frac{1}{\varepsilon_p^k} \tag{47}$$

and

$$r_0^k = \left(\frac{\sigma^k - \sigma^{k-1}}{\varepsilon_p^k - \varepsilon_p^{k-1}} - \frac{\sigma^{k+1} - \sigma^k}{\varepsilon_p^{k+1} - \varepsilon_p^k}\right)\varepsilon_p^k \tag{48}$$

as regards the determination of ζ^k and r_0^k. In Eq. (48), σ^k and ε_p^k denote the stress and plastic strain at the kth point on the monotonic stress-plastic strain relations. From Eq. (48), since k ranges from 0 to 10 $(M+1)$, σ^0 denotes the initial yield stress when the initial plastic strain satisfies $\varepsilon_p^0 = 0$.

Determination of the saturated value of r^k requires the cyclic stress–strain curve with regard to the experimental stabilized hysteresis loop. From Eqs. (36) and (37) r^k can be expressed as

$$r^k = r_0^k + r_{\Delta s}^k[1 - a_1^k e^{-b_1^k p} - (1 - a_1^k)e^{-b_2^k p}], \tag{49}$$

Moreover, since Fang and Sun [59,60] reasonably identify the independence between a_1^k, b_1^k, b_2^k and k, the parameters can be determined by

$$1 - \frac{\sigma_\text{peak} - \sigma_\text{peak,min}}{\sigma_\text{peak,max} - \sigma_\text{peak,min}} = 1 - a_1 e^{-b_1 p} - (1 - a_1)e^{-b_2 p}, \tag{50}$$

from the cyclic stress–strain curve [59]. In Eq. (50), σ_peak denotes the peak stress of the identified stable hysteresis loops. $\sigma_\text{peak,min}$ and $\sigma_\text{peak,max}$ are corresponding minimum and maximum values of σ_peak, respectively.

In processing, the calculated cyclic stress–strain curve was divided into $M = 9$ segments, which was considered reasonable enough, as reported in [59,60]. Generally, the parameters on describing the elastoplastic behavior of SS304 are summarized in Table 2.

In this study, ABAQUS was used to simulate the mechanical behavior of thin-walled tubular specimen machined from SS304 authentic steel. ABAQUS is an advanced general nonlinear finite element analysis software, which has a very obvious advantage in solving nonlinear problems as well as power user support by user defined material subroutine (UMAT) written in FORTRAN program language.

4. Critical plane-based multiaxial fatigue criteria

4.1. Critical plane method

Variation of stress principal axis of components subjected to multiaxial fatigue loads brings a lot of confusion to the understanding of multiaxial failure mechanism, that is the conventional uniaxial fatigue models fail to directly apply to the multiaxial fatigue life assessment. Therefore, the critical plane method was developed by Brown and Miller [4], which focused on this critical plane and blamed the failure of components subjected to multiaxial fatigue loads on the accumulation of damage indicators on a specified plane, namely the critical plane. This is a reliable way to simplify the multiaxial difficulty into the uniaxial issue reasonably. Based on the assumption, life prediction models of uniaxial fatigue can be introduced into the evaluation of multiaxial fatigue. Most of the subsequent studies were based on the critical plane method and various criteria were developed. According to the characteristics of damage parameters, stress criteria, strain criteria, stress/strain criteria, and energy criteria can be distinguished, as listed in Table 1.

In this paper, seven typical criteria (Findley criterion [3], Brown Miller criterion [4], Fatemi Socie criterion [11], Wang–Brown criterion [5], Smith–Watson–Topper criterion [12], Liu-I and Liu-II criteria [15]) were selected to predict the multiaxial fatigue life of specimens machined from SS304, and the multiaxial fatigue lives predicted by various criteria were compared with the new proposed shear/normal strain energy ratio-based (SNSER) criterion in this paper.

4.2. Findley criterion

Findley [3] defined a linear combination of the shear stress amplitude and the normal stress to model the fatigue damage. The damage indicator developed by Findley fails to meet the concept of the critical plane method, which is defined as one or more planes within a material subject to a maximum value of the damage indicator. After some researchers introduced the damage indicator into Basquin's equation to describe the shear-mode cracking, the Findley model was finally grafted into the multiaxial field, as

$$\left(\frac{\Delta\tau}{2} + \kappa_\text{F}\sigma_\text{n}\right)_\text{max} = \tau_\text{f}'(2N_\text{f})^{b'}, \tag{51}$$

4.3. Brown Miller criterion

Brown and Miller [4] proposed the critical plane method, which considers that fatigue crack growth is controlled by two parameters, one is the maximum shear strain amplitude, the other is the normal strain on the plane where the maximum shear strain is located. These two parameters satisfy the following relationships

$$\frac{\gamma_{\max}}{2}+\kappa_{\mathrm{BM}}\Delta\varepsilon_{\mathrm{n}}=A\frac{\sigma_{\mathrm{f}}'}{E}(2N_{\mathrm{f}})^{b}+B\varepsilon_{\mathrm{f}}'(2N_{\mathrm{f}})^{c}, \tag{52}$$

where $A=1.3+0.7\kappa_{\mathrm{BM}}$, $B=1.5+0.5\kappa_{\mathrm{BM}}$ with κ_{BM} is the material dependent parameter represents the effect of normal strain on cracks parallel to the critical plane.

4.4. Fatemi Socie criterion

Fatemi and Socie [11] further revised Brown–Miller's expression, believing that the normal stress dominates the crack parallel to the critical plane, so the expression is as follows

$$\frac{\Delta\gamma}{2}\left(1+\kappa_{\mathrm{FS}}\frac{\sigma_{\mathrm{n,max}}}{\sigma_{\mathrm{y}}}\right)=\frac{\tau_{\mathrm{f}}'}{G}(2N_{\mathrm{f}})^{b'}+\gamma_{\mathrm{f}}'(2N_{\mathrm{f}})^{c'}, \tag{53}$$

where κ_{FS} is the sensitivity parameter which is related to the tensile and torsional properties of materials and varies with fatigue life, that is

$$\kappa_{\mathrm{FS}}=\frac{\kappa_{\mathrm{FS},0}\sigma_{\mathrm{y}}}{\sigma_{\mathrm{f}}'(2N_{\mathrm{f}})^{b}}, \tag{54}$$

with

$$\kappa_{\mathrm{FS},0}=\frac{\frac{\tau_{\mathrm{f}}'}{G}(2N_{\mathrm{f}})^{b'}+\gamma_{\mathrm{f}}'(2N_{\mathrm{f}})^{c'}}{(1+\nu_{\mathrm{e}})\frac{\sigma_{\mathrm{f}}'}{E}(2N_{\mathrm{f}})^{b}+(1+\nu_{\mathrm{p}})\varepsilon_{\mathrm{f}}'(2N_{\mathrm{f}})^{c}}-1. \tag{55}$$

4.5. Wang-Brown criterion

Wang and Brown [5] developed a multiaxial damage model based on the multiaxial counting cycle method and considered the effects of shear strain and average stress on multiaxial fatigue life.

$$\frac{\Delta\gamma_{\max}}{2}+\kappa_{\mathrm{WB}}\frac{\Delta\varepsilon_{\mathrm{n}}}{2}=A\frac{\sigma_{\mathrm{f}}'-2\sigma_{\mathrm{n,mean}}}{E}(2N_{\mathrm{f}})^{b}+B\varepsilon_{\mathrm{f}}'(2N_{\mathrm{f}})^{c}, \tag{56}$$

where $A=(1+\nu_{\mathrm{e}})+(1-\nu_{\mathrm{e}})\kappa_{\mathrm{WB}}$, $B=(1+\nu_{\mathrm{p}})+(1-\nu_{\mathrm{p}})\kappa_{\mathrm{WB}}$ and ν_{e} and ν_{p} are the Poisson's ratios of material under elastic and plastic conditions (usually $\nu_{\mathrm{p}}=0.5$) respectively. $\sigma_{\mathrm{n,mean}}$ is the average normal stress in the plane of maximum shear strain (the critical plane).

4.6. Smith–Watson–Topper criterion

The Smith Waston and Topper (SWT) damage criterion [12] with a critical plane is popular in multiaxial loading. This method was developed for materials failing predominately in crack propagation on planes of maximum tensile strain or stress. In materials, crack initiation in shear, bur early life is controlled by crack propagation on planes perpendicular to the maximum principal stress and strain. Bannantine [13] extended the uniaxial SWT model to multiaxial concept. Meanwhile, Socie [1] introduced the critical plane concept into the SWT parameter for analyzing both proportional and non-proportional situations. This model is express as

$$\frac{\Delta\varepsilon}{2}\sigma_{\mathrm{n,max}}=\frac{\sigma_{\mathrm{f}}'^{2}}{E}(2N_{\mathrm{f}})^{2b}+\sigma_{\mathrm{f}}'\varepsilon_{\mathrm{f}}'(2N_{\mathrm{f}})^{2c}, \tag{57}$$

Table 3
Chemical composition of SS304 (wt. %) in the research.

Fe	C	Si	Mn	P	S	Cr	Ni
Balanced	0.04	0.41	1.05	0.035	0.003	17.1	8.1

4.7. Liu-I and Liu-II criteria

Liu [15] proposed a multiaxial fatigue life prediction method based on the virtual tensile strain energy theory. The theory is also based on the critical plane method. The total strain energy that causes material failure can be decoupled into the virtual tensile strain energy and the virtual shear strain energy. Thus, two life prediction methods with different physical meanings are derived. The maximum virtual tensile strain energy (Liu I) theory dominated by tensile failure and the maximum virtual shear strain energy (Liu II) theory dominated by shear failure are respectively. The two methods are expressed as follows.

Liu I:

$$(\Delta\sigma_{\mathrm{n}}\Delta\varepsilon_{\mathrm{n}})_{\max}+(\Delta\tau\Delta\gamma)=\frac{4\sigma_{\mathrm{f}}'^{2}}{E}(2N_{\mathrm{f}})^{2b}+4\sigma_{\mathrm{f}}'\varepsilon_{\mathrm{f}}'(2N_{\mathrm{f}})^{b+c} \tag{58}$$

Liu II:

$$(\Delta\sigma_{\mathrm{n}}\Delta\varepsilon_{\mathrm{n}})+(\Delta\tau\Delta\gamma)_{\max}=\frac{4\tau_{\mathrm{f}}'^{2}}{G}(2N_{\mathrm{f}})^{2b'}+4\tau_{\mathrm{f}}'\gamma_{\mathrm{f}}'(2N_{\mathrm{f}})^{b'+c'} \tag{59}$$

4.8. Proposed shear/normal strain energy ratio-based (SNSER) criterion

Combining the newly proposed SNSER criterion and the concept of the critical plane, the equivalent total strain energy $\hat{M}_{\mathrm{eq}}$ can be given as

$$\begin{aligned}\hat{M}_{\mathrm{eq,max}}&=(1+\kappa\Phi_{\mathrm{YS}})\left[\alpha\Delta\sigma\Delta\varepsilon+(1-\alpha)\Delta\tau\Delta\gamma\right]_{\max}\\&=\frac{4\sigma_{\mathrm{f}}'^{2}}{E}(2N_{\mathrm{f}})^{2b}+4\sigma_{\mathrm{f}}'\varepsilon_{\mathrm{f}}'(2N_{\mathrm{f}})^{b+c}\\&\text{or}=\frac{6}{1+\nu_{\mathrm{e}}}\frac{\tau_{\mathrm{f}}'^{2}}{G}(2N_{\mathrm{f}})^{2b'}+4\tau_{\mathrm{f}}'\gamma_{\mathrm{f}}'(2N_{\mathrm{f}})^{b'+c'}.\end{aligned} \tag{60}$$

where the subscript max denotes that structural failure occurs at the location of maximum total energy.

5. Experiments

The austenitic stainless steel 304 (SS304), a face-centered cubic structure (FCC), with chromium (chemical) content up to 17% and nickel (chemical) content about 8%, was studied in this paper and presented in Table 3. The raw material was cut by electrical discharge machining (EDM) which was solution treated at 1050 °C for 30 min and water-cooled. The microstructure of SS304 is available in Fig. 5, which clearly illustrates the grain size of SS304 that ranges from 100 to 150 μm.

The experimental data on the mechanical properties of SS304 material in this article are from [59,64]. As reported, four types of tests were carried out at room temperature, including (1) monotonic tensile test, (2) axial fatigue test [59,64], (3) torsional fatigue test [59,64], (3) multiaxial fatigue test (12 paths from [59] and 47 paths from [64], respectively). All experimental conditions and load spectrum are also available in the references.

6. Results and discussion

6.1. Determination of fatigue parameters

Fig. 6 shows the engineering stress/strain curve during the monotonic tensile process. Morphology of the necking to fracture of the specimen is also shown in Fig. 6. Therefore, monotonic parameters can be acquired and presented in Table 4. Yang et al. [65] developed a life prediction method to determine the fatigue parameters (σ_{f}', $\varepsilon_{\mathrm{f}}'$,

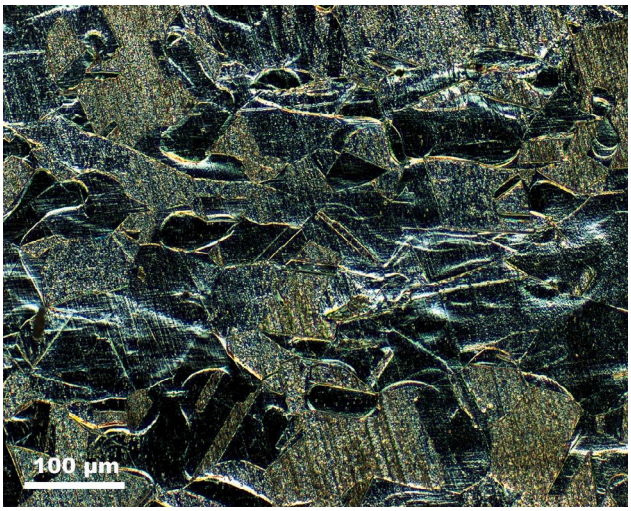

Fig. 5. The microstructure of SS304 (200×, observed by polarizer).

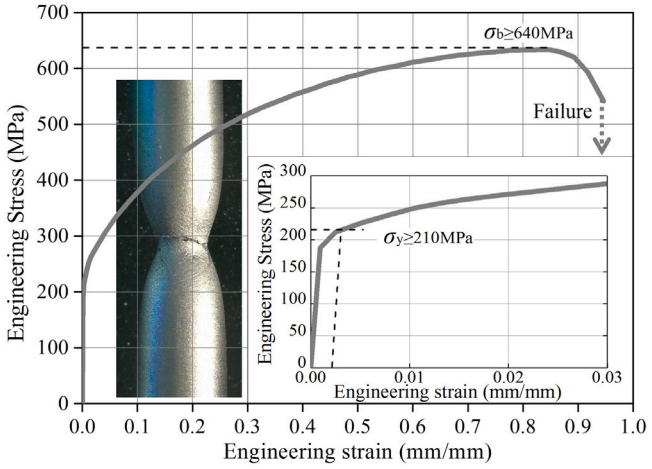

Fig. 6. The monotonic tensile curve of SS304.

Table 4
Monotonic/cyclic and fatigue parameters of SS304 in the research.

Monotonic/cyclic parameters			
σ_b/MPa	σ_y/MPa	E/GPa	K'/MPa
680	220	198	1660
ψ	δ	ν_e	n'
0.74	0.94	0.3	0.297
Fatigue parameters ($R = -1$)			
σ_f'/MPa	b	ε_f'	c
798	−0.102	1.05	−0.614
τ_f'/MPa	b'	γ_f'	c'
461	−0.102	1.805	−0.614

b and c) in total strain life equation based on the monotonic tensile parameters. This study introduced this method to determine the fatigue parameters of SS304 efficiently, the value of which is also presented in Table 4. Substituting the new determined uniaxial fatigue parameters into Eq. (9), the shear fatigue parameters (τ_f', γ_f', b' and c') can be subsequently obtained and presented in Table 4.

The accuracy of the method proposed in [41–43], that is, determining shear fatigue parameters from uniaxial fatigue parameters, needs to be verified. Accordingly, uniaxial/torsional fatigue life curves are plotted in Fig. 7 and highlighted in purple and pink, respectively. [59,64] provided the uniaxial/torsional fatigue test data of SS304. The

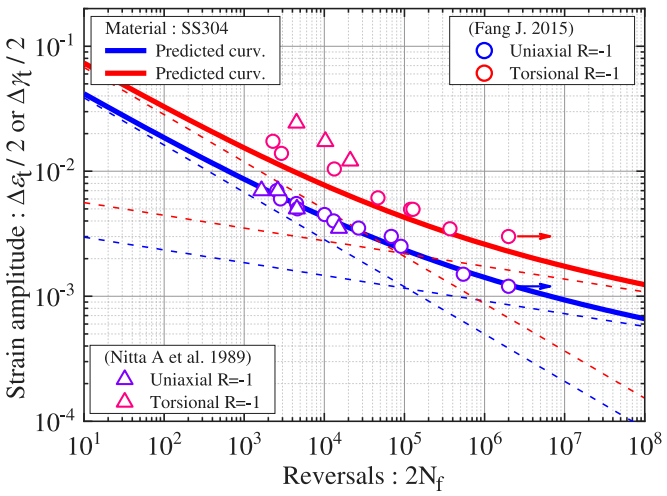

Fig. 7. Verification of methods proposed in [41–43] on predicting uniaxial/torsional fatigue life of SS304 provided in [59,64].

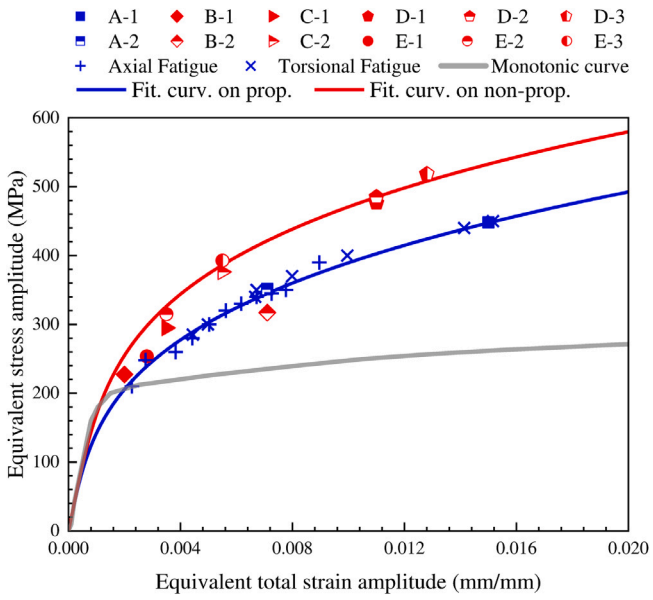

Fig. 8. Experimental results for SS304 under proportional and non-proportional loadings.

comparison between the predicted and tested fatigue life shows that the method provided in [41–43] provided tolerable life prediction accuracy of SS304.

The elastoplastic behavior of SS304 subjected to various loadings paths are presented in Fig. 8. The relationship between stress and strain for monotonic tensile tests and uni-/multi-axial fatigue tests were available in this figure. Both cyclic hardening and non-proportionality additional hardening behavior were clearly illustrated. The Ramberg–Osgood model was used to describe the cyclic stress–strain relationship

$$\frac{\Delta\varepsilon_{eq}}{2} = \frac{\Delta\sigma_{eq}}{2E} + \left(\frac{\Delta\sigma_{eq}}{2K'}\right)^{1/n'}, \tag{61}$$

where K' and n' are cyclic strain hardening coefficient and cyclic strain hardening exponent, respectively. For uniaxial/proportional multiaxial fatigue tests, K' = 1660 MPa, n' = 0.297 (Table 4) and for non-proportional multiaxial fatigue tests, K' = 1660 MPa, n' = 0.258. $\Delta\varepsilon_{eq}/2$ and $\Delta\sigma_{eq}/2$ are the equivalent total strain amplitude and the equivalent

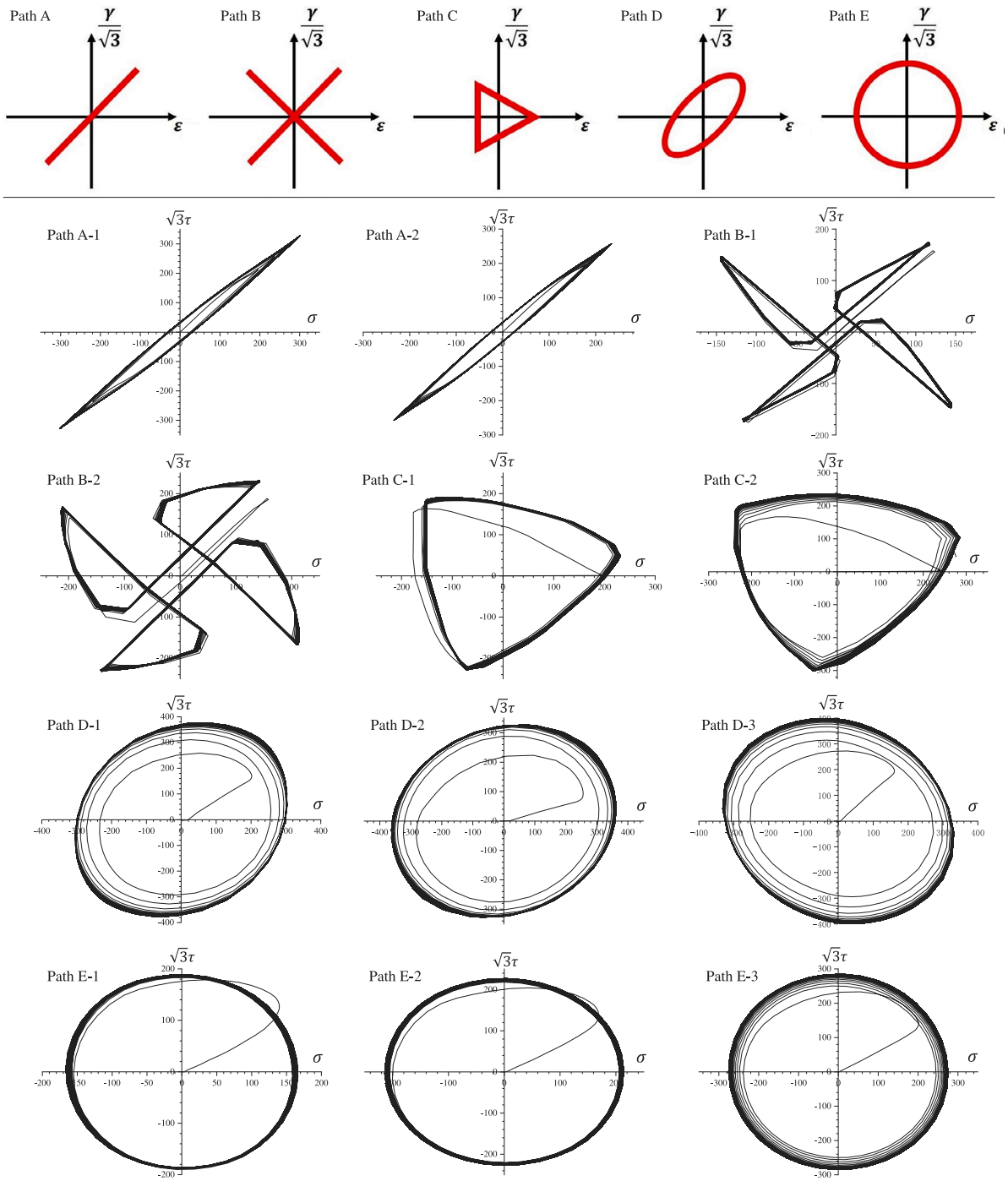

Fig. 9. Strain paths (red marked) in multiaxial fatigue tests and stress paths (black marked) namely calculated hysteresis loops. (For interpretation of the references to color in this figure legend, the reader is referred to the web version of this article.)

stress amplitude, respectively, which can be given in mathematical expressions as [66]

$$\begin{cases} \dfrac{\Delta\sigma_{\mathrm{eq}}}{2} = \mathrm{Min}\left\{\mathrm{Max}\left[\sqrt{\dfrac{3}{2}(s_{ij}-s_{ij}^{0})(s_{ij}-s_{ij}^{0})}\right]\right\}, \\ \dfrac{\Delta\varepsilon_{\mathrm{eq}}}{2} = \mathrm{Min}\left\{\mathrm{Max}\left[\sqrt{\dfrac{3}{2}(\varepsilon_{ij}-\varepsilon_{ij}^{0})(\varepsilon_{ij}-\varepsilon_{ij}^{0})}\right]\right\}, \end{cases} \tag{62}$$

where s_{ij} and ε_{ij} are the deviatoric stress tensor and the strain tensor, respectively; s_{ij}^{0} and ε_{ij}^{0} denotes the center of the minimum circle in the deviatoric stress and strain space, respectively.

6.2. Multiaxial fatigue life prediction

In this study, multiaxial fatigue performance including various proportional and non-proportional loading paths was predicted. As shown in Fig. 9, the red marked lines indicate the applied strain loading paths controlled by tension/torsion dual-channel extensometer in the multiaxial fatigue tests. The strain controlled paths studied includes (1) one-way proportional tension/torsion (Path A), (2) dual-way proportional tension/torsion (Path B), (3) right-pointed triangle mix-mode (Path C), (4) ellipse mix-mode (Path D), (5) circular mix-mode (Path E). To note that, Path B, namely the dual-way proportional tension/torsion

Table 5
Comparison of calculated non-proportionalities and tensile/shear energy ratios for various kinds of loading paths.

	Paths	Φ	α	Paths	Φ	α	Paths	Φ	α
12 kinds [59]	Path A-1	0.0418	0.4528	Path C-1	0.5917	0.5109	Path D-3	0.7668	0.2186
	Path A-2	0.0450	0.4505	Path C-2	0.6622	0.5318	Path E-1	0.8459	0.4631
	Path B-1	0.1265	0.4304	Path D-1	0.7597	0.4103	Path E-2	0.9192	0.4791
	Path B-2	0.3230	0.4436	Path D-2	0.8366	0.7426	Path E-3	0.9531	0.4821
47 kinds [64]	Path 1	0	1.0000	Path 17	0.04	0.0524	Path 33	0.8367	0.2646
	Path 2	0	1.0000	Path 18	0.04	0.0528	Path 34	0.8246	0.2677
	Path 3	0	1.0000	Path 19	0.04	0.0519	Path 35	0.8173	0.2714
	Path 4	0	1.0000	Path 20	0.04	0.0519	Path 36	0.7914	0.2255
	Path 5	0.04	0.2474	Path 21	0	0.0000	Path 37	0.7907	0.2283
	Path 6	0.04	0.2474	Path 22	0	0.0000	Path 38	0.7881	0.2312
	Path 7	0.04	0.2473	Path 23	0	0.0000	Path 39	0.7059	0.1352
	Path 8	0.04	0.2477	Path 24	0.6098	0.3179	Path 40	0.6940	0.1355
	Path 9	0.04	0.2036	Path 25	0.5943	0.3163	Path 41	0.6979	0.1377
	Path 10	0.04	0.2036	Path 26	0.5688	0.3125	Path 42	0.6414	0.0577
	Path 11	0.04	0.2030	Path 27	0.6737	0.3172	Path 43	0.7080	0.0754
	Path 12	0.04	0.2021	Path 28	0.7087	0.3168	Path 44	0.5704	0.0765
	Path 13	0.04	0.2021	Path 29	0.6889	0.3176	Path 45	0.4277	0.0200
	Path 14	0.04	0.1066	Path 30	0.7193	0.3027	Path 46	0.3518	0.0190
	Path 15	0.04	0.1069	Path 31	0.7810	0.3061	Path 47	0.3268	0.0191
	Path 16	0.04	0.1051	Path 32	0.7637	0.3072			

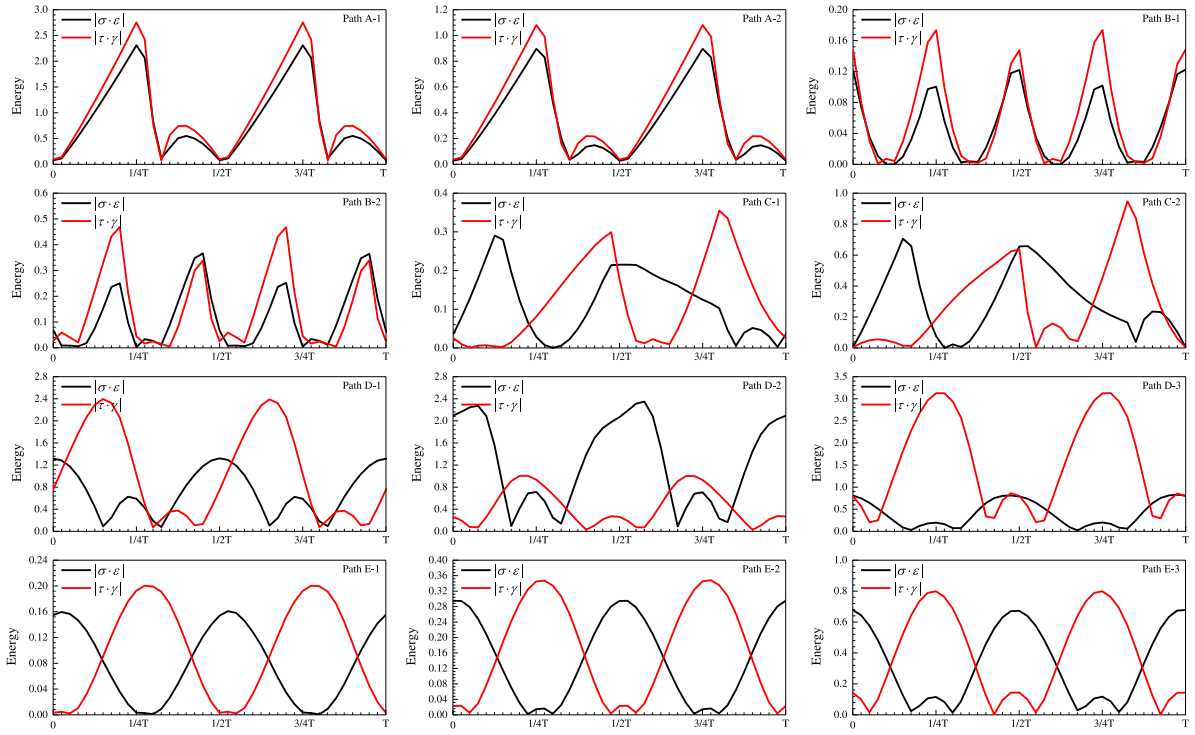

Fig. 10. Energy evolution of different paths in a loading cycle under the condition of cyclic stability.

loading path was clarified into the non-proportional category. Accordingly, the calculated hysteresis loops of the above paths during the whole cyclic loading process are also available in Fig. 9, in which the elastoplastic behavior of SS304 subjected to proportional and non-proportional loads is completely illustrated. In light of the definition of the non-proportionality (Φ), schematically and quantitatively described in Fig. 4 and Eq. (24) respectively. It is, therefore, eventually to identify and compare the non-proportionalities of 12 different loading paths in Table 5. Furthermore, all paths were elaborate to correlate the normal strain energy and shear strain energy against running time in the stable cycle and shown in Fig. 10. According to the expressions of Eqs. (16) and (17), the energy weight coefficient for various loading paths can also be acquired and presented in Table 5.

Comparison of predicted and tested fatigue life for 7 typical criteria and the new proposed criterion are shown in Fig. 11. Basically, the Fatime-Socie (Fig. 11(b)), Liu (Fig. 11(f) and (g)) and new criteria (Fig. 11(h)) give accurate life predictions for multiaxial fatigue under both proportional and non-proportional loads, most of which are within the life factor-of-five bands. Among the whole criteria, the new criterion gives the best life prediction performance. Except for a slightly conservative case, all the predicted lives are within the life factor of two bands (Fig. 11(h)). Furthermore, a comparison of predicted and experimental multiaxial fatigue life of all criteria are available in Fig. 12(a). It is clearly confirmed that the predicted multiaxial fatigue life SS304 subjected to proportional and non-proportional loads of the new criterion is of satisfying accuracy and tends to be conservative.

Moreover, Nitta et al. gave the multiaxial fatigue behavior of 304 stainless steel in the medium life stage [64]. In their study, fatigue performance of SS304 with regard to 47 different kinds of uniaxial/multiaxial fatigue paths was carried out. Accordingly, based on

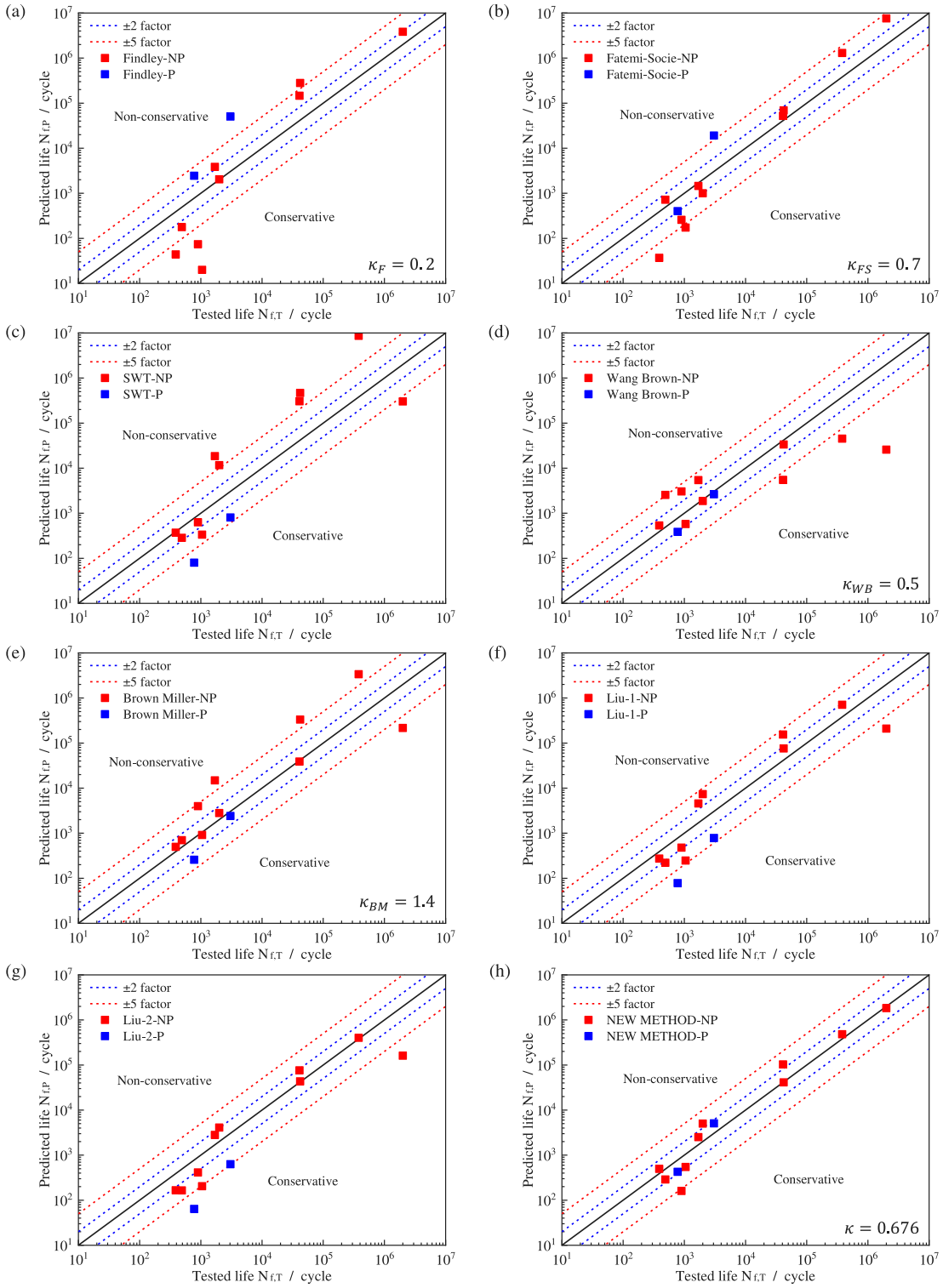

Fig. 11. Fatigue life prediction by (a) Findley, (b) Fatemi Socie, (c) SWT, (d) Wang–Brown, (e) Brown–Miller, (f) Liu-1, (g) Liu-2, (h) New criterion.

the constitutive model we performed and programmed, the tensile and shear stress states under the specified loading paths in [64] are calculated and the numerically stable hysteresis loops are presented in Fig. 13, among which the purple and pink highlighted represent the proportional and non-proportional loading paths, respectively. From numerically stable hysteresis loops in Fig. 13, calculated non-proportionalities and tensile/shear energy ratios for as-mentioned 47 kinds of loading paths are also available in Table 5. Finally, the multiaxial fatigue life of SS304 provided by Nitta et al. under 47 loading paths are predicted by the newly proposed method and shown in Fig. 11(b). In this figure, the purple and pink highlighted data represent proportional and non-proportional loading conditions respectively. As presented, almost all the predicted results are within the life factor-of-five bands.

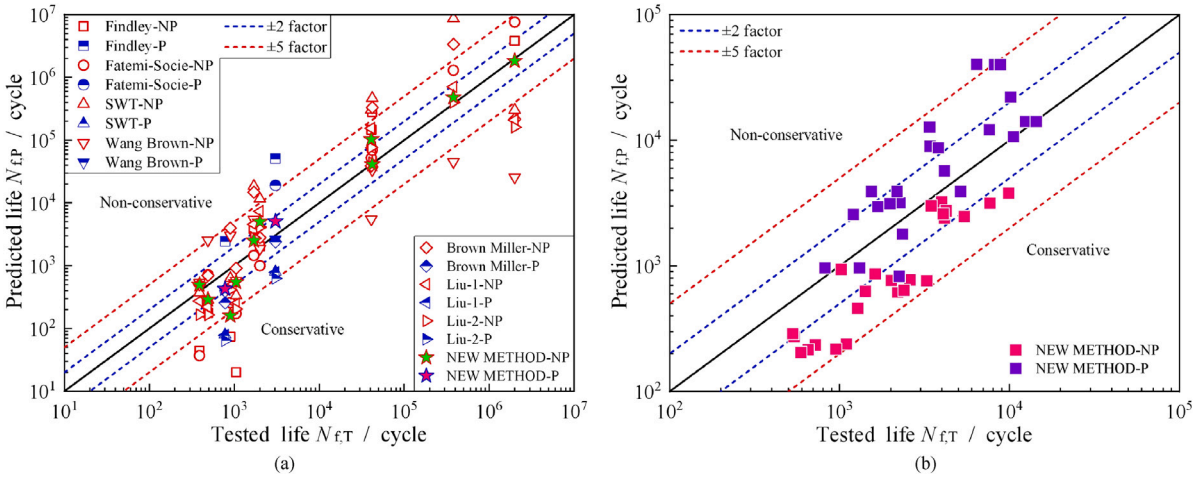

Fig. 12. Comparison of predicted and experimental multiaxial fatigue life: (a) All as-mentioned criteria for 12 paths in [59]; (b) New proposed criterion for 47 paths in [64].

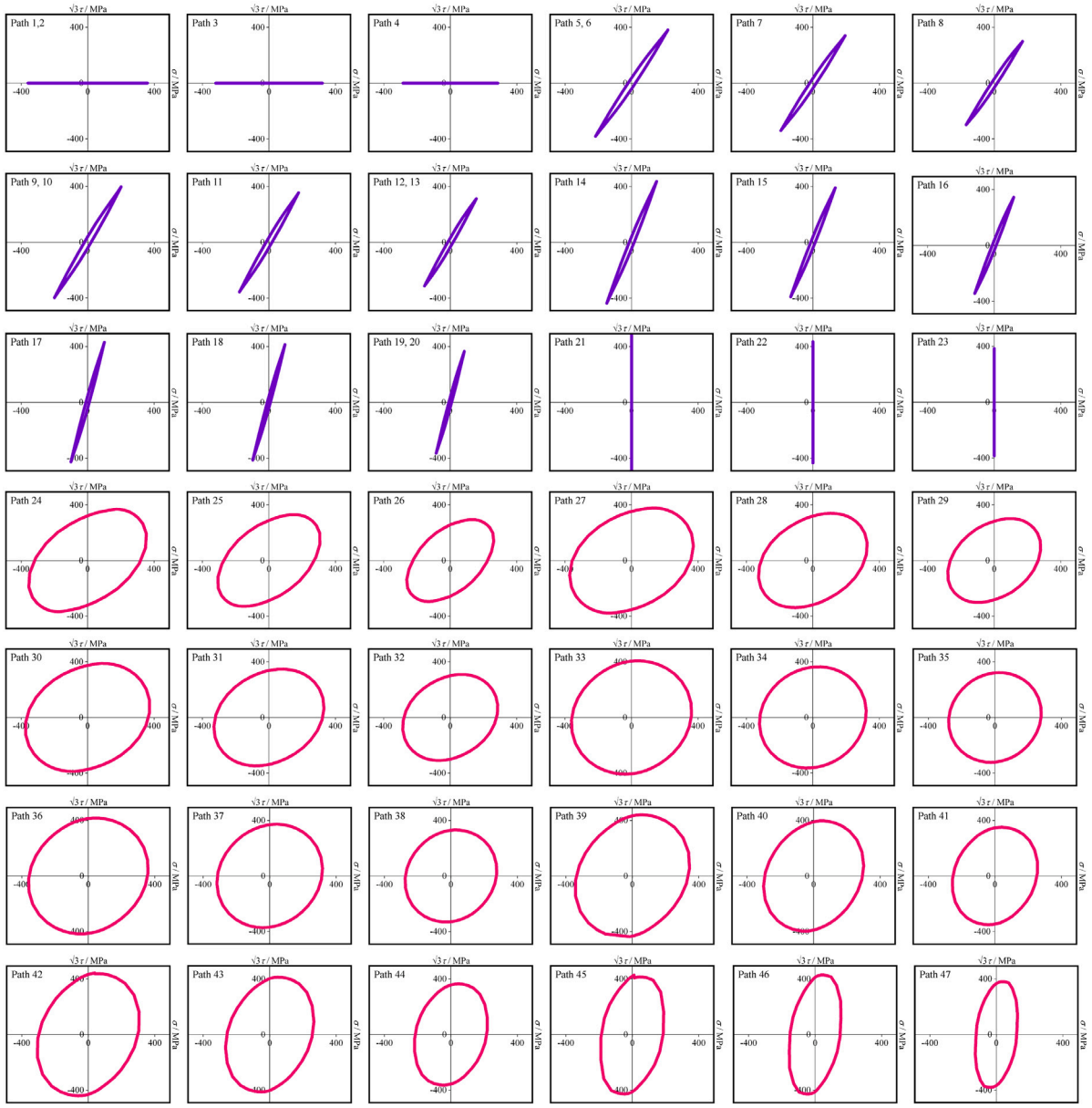

Fig. 13. Calculated hysteresis loops, among which the purple and pink highlighted represent the proportional and non-proportional loading paths, respectively.

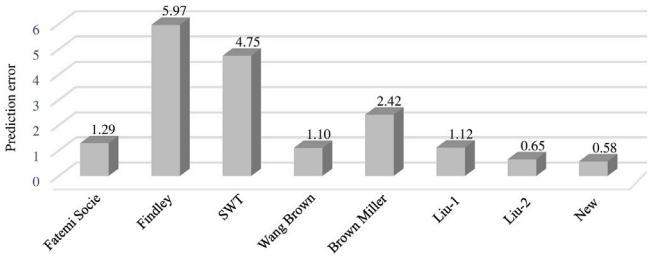

Fig. 14. Prediction errors with different criteria.

6.3. Prediction error evaluation

In this paper, evaluation and quantitative comparison among various criteria on 12 kinds of loading paths illustrated in Fig. 9 were carried out. In order to quantitatively evaluate the accuracy and reliability of various multiaxial fatigue criteria, the evaluation value based on the error criterion, *Error*, was defined by Park and Jeon et al. [67–69] and applied in some investigations [6,36]. The prediction error can be expressed as follows

$$Error = \frac{\sum_1^P \frac{N_{f,P} - N_{f,T}}{N_{f,T}}}{P}, \tag{63}$$

where $P = 12$ is the number of paths mentioned in Fig. 9, $N_{f,P}$ is the predicted fatigue life and $N_{f,T}$ is the tested fatigue life. The prediction error *Error* against various multiaxial fatigue criteria is presented in Fig. 14. As it is shown in Fig. 14, for all loading paths, the prediction error of the stress-dependent Findley criterion and the energy-dependent SWT criterion are obvious, both of which are more than 4. While the Fatemi-Socie, Wang–Brown and Liu's criteria acquired satisfied life prediction results with fairly small error and their values are less than 2. Generally, the novel method developed in this paper provides the minimum prediction error in comparison with the other criteria.

7. Conclusions

(1) In this work, a novel energy-based multiaxial fatigue criterion was proposed considering the effect of both normal and shear strain energy. The stress/strain-path-dependent energy weight coefficient was introduced to the criterion considering the different contributions of the energy components.
(2) A newly defined non-proportionality based on the stable hysteresis loops was also introduced to the new criterion considering the non-proportional additional hardening behavior during the multiaxial loading process.
(3) Most of the coefficients (fatigue parameters and non-proportional additional hardening factor) in the new criterion can be determined by monotonic tensile parameters, which improved the applicability and feasibility of multiaxial fatigue life prediction.
(4) The performance of the new criterion was approved by comparing the predicted and tested life of SS304 by various kinds of multiaxial loading paths and most of the predicted fatigue life falls within factor-of-two bands.

Declaration of competing interest

The authors declare that they have no known competing financial interests or personal relationships that could have appeared to influence the work reported in this paper.

Acknowledgment

The present work is financed by the National Natural Science Foundation of China under the contract number 12002185.

References

[1] Socie DF. Multiaxial fatigue damage models. Key Eng Mater 1987;109(4):293.
[2] Stephens R, Fatemi A, Stephens R, Fuchs H. Metal fatigue in engineering. 2000.
[3] Findley WM. Theory for the effect of mean stress on fatigue of metals under combined torsion and axial load or bending. J Eng Ind 1959;81(6):301–6.
[4] Brown MW, Miller KJ. A theory for fatigue failure under multiaxial stress-strain conditions. Proc Inst Mech Eng 1973;187:745–55.
[5] Wang CH, Brown MW. Life prediction techniques for variable amplitude multiaxial fatigue—Part 1: Theories. J Eng Technol 1996;118(3):367–70.
[6] Li J, Zhang Z, Sun Q, Li C. Multiaxial fatigue life prediction for various metallic materials based on the critical plane approach. Int J Fatigue 2011;33:90–1101.
[7] Ince A, Glinka G. A generalized fatigue damage parameter for multiaxial fatigue life prediction under proportional and non-proportional loadings. Int J Fatigue 2014;62:34–41.
[8] Ince A, Glinka G. Innovative computational modeling of multiaxial fatigue analysis for notched components. Int J Fatigue 2016;82:134–45.
[9] Zhong B, Wang Y, Wei D, Wang J. A new life prediction model for multiaxial fatigue under proportional and non-proportional loading paths based on the pi-plane projection. Int J Fatigue 2017;102:241–51.
[10] Zhong B, Wang Y, Wei D, Zhang K, Wang J. Multiaxial fatigue life prediction for powder metallurgy superalloy FGH96 based on stress gradient effect. Int J Fatigue 2018;109:26–36.
[11] Fatemi A, Socie DF. A critical plane approach to multiaxial fatigue damage including out of plane loading. Fatigue Fract Eng Mater Struct 1988;11(3):149–65.
[12] Smith K, Watson P, Topper T. A stress strain parameter for the fatigue of metals. J Mater 1970;5:767–78.
[13] Bannantine J, Socie D. A variable amplitude multiaxial fatigue life prediction method. In: Fatigue under biaxial and multiaxial loading. 1989, p. 35–51.
[14] Ellyin F. Fatigue (multiaxial): General. In: Buschow KJ, Cahn RW, Flemings MC, Ilschner B, Kramer EJ, Mahajan S, Veyssière P, editors. Encyclopedia of materials: Science and technology. Oxford: Elsevier; 2001, p. 2939–43.
[15] Liu K. Method based on virtual strain-energy parameters for multiaxial fatigue life prediction, Vol. 1191. ASTM STP 1191, 1993, p. 67–84.
[16] Chu C-C, Conle A, Bonnen J. Multiaxial stress-strain modelling and fatigue life prediction of SAE axle shafts, Vol. 1191. ASTM STP 1191, 1993, p. 37–54.
[17] Chen X, Xu S, Huang D. A critical plane-strain density criterion for multiaxial low-cycle fatigue life under non-proportional loading. Fatigue Fract Eng Mater Struct 1999;22:679–86.
[18] Yanyao J. A fatigue criterion for general multiaxial loading. Fatigue Fract Eng Mater Struct 2000;23:19–32.
[19] Jiang Y, Hertel O, Vormwald M. An experimental evaluation of three critical plane multiaxial fatigue criteria. Int J Fatigue 2007;29(8):1490–502.
[20] Yu Q, Zhang J, Jiang Y, Li Q. Multiaxial fatigue of extruded AZ61A magnesium alloy. Int J Fatigue 2011;33(3):437–47.
[21] Varvani-Farahani A. A new energy-critical plane parameter for fatigue life assessment of various metallic materials subjected to in-phase and out-of-phase multiaxial fatigue loading conditions. Int J Fatigue 2000;22(4):295–305.
[22] Varvani-Farahani A, Sharma M, Kianoush M. Fatigue damage analysis and life assessment under variable amplitude loading conditions. Mater Sci Eng A 2005;403(1):42–7.
[23] Varvani-Farahani A, Kianoush M, Sharma M. Fatigue failure assessment of engineering components under service loading conditions. Mater Des 2007;28(2):575–80.
[24] Lazzarin P, Livieri P, Berto F, Zappalorto M. Local strain energy density and fatigue strength of welded joints under uniaxial and multiaxial loading. Eng Fract Mech 2008;75(7):1875–89.
[25] Radaj D, Berto F, Lazzarin P. Local fatigue strength parameters for welded joints based on strain energy density with inclusion of small-size notches. Eng Fract Mech 2009;76(8):1109–30.
[26] Berto F, Elices M, Lazzarin P, Zappalorto M. Fracture behaviour of notched round bars made of PMMA subjected to torsion at room temperature. Eng Fract Mech 2012;90:143–60.
[27] Lagoda T ME. Generalization of energy-based multiaxial fatigue criteria to random loading. In: Kalluri S, Bonacuse PJ, editors. Mutiaxial fatigue and deformation: testing and prediction, Vol. 1387. ASTM STP 1387, 2000, p. 173–90.
[28] Łagoda T, Ogonowski P. Criteria of multiaxial random fatigue based on stress, strain and energy parameters of damage in the critical plane. Materwiss Werksttech 2005;36(9):429–37.
[29] Kardas D, Kluger K, Łagoda T, Ogonowski P. Fatigue life of aluminium alloy 2017(a) under proportional constant amplitude bending with torsion in energy approach. Mater Sci - Mater Sci-Engl TR 2008;44:541–9.
[30] Walat K, Kurek M, Ogonowski P, Łagoda T. The multiaxial random fatigue criteria based on strain and energy damage parameters on the critical plane for the low-cycle range. Int J Fatigue 2012;37:100–11.
[31] Zhu H, Wu H, Lu Y, Zhong Z. A novel energy-based equivalent damage parameter for multiaxial fatigue life prediction. Int J Fatigue 2019;121:1–8.

[32] Branco R, Costa J, Berto F, Antunes F. Fatigue life assessment of notched round bars under multiaxial loading based on the total strain energy density approach. Theor Appl Fract Mech 2018;97:340–8.
[33] Branco R, Prates P, Costa J, Berto F, Kotousov A. New methodology of fatigue life evaluation for multiaxially loaded notched components based on two uniaxial strain-controlled tests. Int J Fatigue 2018;111:308–20.
[34] Branco R, Prates P, Costa J, Borrego L, Berto F, Kotousov A, Antunes F. Rapid assessment of multiaxial fatigue lifetime in notched components using an averaged strain energy density approach. Int J Fatigue 2019;124:89–98.
[35] Lu C, Melendez J, Martínez-Esnaola J. Fatigue damage prediction in multiaxial loading using a new energy-based parameter. Int J Fatigue 2017;104:99–111.
[36] Lu C, Melendez J, Martínez-Esnaola J. Modelling multiaxial fatigue with a new combination of critical plane definition and energy-based criterion. Int J Fatigue 2018;108:109–15.
[37] You B-R, Lee S-B. A critical review on multiaxial fatigue assessments of metals. Int J Fatigue 1996;18(4):235–44.
[38] Macha E SC. Energy criteria of multiaxial fatigue failure. Fatigue Fract Eng Mater Struct 1999;22(12):1053–70.
[39] Karolczuk A ME. A review of critical plane orientations in multiaxial fatigue failure criteria of metallic materials. Int J Fract 2005;134(3):267–304.
[40] Fatemi A, Shamsaei N. Multiaxial fatigue: An overview and some approximation models for life estimation. Int J Fatigue 2011;33(8):948–58.
[41] Socie DF, Marquis GB. Multiaxial fatigue. Warrendale (PA): SAE; 2000.
[42] Susmel L, Meneghetti G, Atzori B. A simple and efficient reformulation of the classical manson–coffin curve to predict lifetime under multiaxial fatigue loading—Part II: Notches. J Eng Mater-T 2009;131(2):021010.
[43] Zhu S, Foletti S, Beretta S. Probabilistic framework for multiaxial LCF assessment under material variability. Int J Fatigue 2017;103:371–85.
[44] Itoh T, Chen X, Nakagawa T, Sakane M. A simple model for stable cyclic stress-strain relationship of type 304 stainless steel under nonproportional loading. J Eng Mater Technol ASME 2000;122:1–9.
[45] Liu Y, Mahadevan S. Strain-based multiaxial fatigue damage modelling. Fatigue Fract Eng Mater Struct 2005;28(12):1177–89.
[46] Itoh T, Yang T. Material dependence of multiaxial low cycle fatigue lives under non-proportional loading. Int J Fatigue 2011;33(8):1025–31.
[47] Wu M, Itoh T, Shimizu Y, Nakamura H, Takanashi M. Low cycle fatigue life of Ti–6Al–4V alloy under non-proportional loading. Int J Fatigue 2012;44:14–20.
[48] Chen X, Gao Q, Sun X-F. Low-cycle fatigue non-proportional loading. Fatigue Fract Eng Mater Struct 2007;19:839–54.
[49] Borodii M, Strizhalo V. Analysis of the experimental data on a low cycle fatigue under nonproportional straining. Int J Fatigue 2000;22(4):275–82.
[50] Meggiolaro MA, de Castro JTP. An improved multiaxial rainflow algorithm for non-proportional stress or strain histories – Part II: The Modified Wang–Brown method. Int J Fatigue 2012;42:194–206.
[51] Araújo J, Dantas A, Castro F, Mamiya E, Ferreira J. On the characterization of the critical plane with a simple and fast alternative measure of the shear stress amplitude in multiaxial fatigue. Int J Fatigue 2011;33(8):1092–100.
[52] Paul SK. Prediction of non-proportional cyclic hardening and multiaxial fatigue life for FCC and BCC metals under constant amplitude of strain cycling. Mater Sci Eng A 2016;656:111–9.
[53] Zhu H, Wu H, Lu Y, Zhong Z. A novel energy-based equivalent damage parameter for multiaxial fatigue life prediction. Int J Fatigue 2019;121:1–8.
[54] Ohno N, Wang JD. Kinematic hardening rules with critical state of dynamic recovery. I - Formulation and basic features for ratchetting behavior. II - Application to experiments of ratchetting behavior. Int J Plast 1993;9(3):375–403.
[55] Chaboche J. A review of some plasticity and viscoplasticity constitutive theories. Int J Plast 2008;24(10):1642–93.
[56] Döring R, Hoffmeyer J, Seeger T, Vormwald M. A plasticity model for calculating stress–strain sequences under multiaxial nonproportional cyclic loading. Comput Mater Sci 2003;28(3):587–96.
[57] Abdel-Karim M. Numerical integration method for kinematic hardening rules with partial activation of dynamic recovery term. Int J Plast 2005;21(7):1303–21.
[58] Kang G, Ohno N, Nebu A. Constitutive modeling of strain range dependent cyclic hardening. Int J Plast 2003;19(10):1801–19.
[59] Jie F. Cyclic plasticity modeling and multiaxial fatigue assessment for an austenitic steel. Herbert Utz Verlag; 2015.
[60] Sun J, Yuan H. Cyclic plasticity modeling of nickel-based superalloy Inconel 718 under multi-axial thermo-mechanical fatigue loading conditions. Int J Fatigue 2019;119:89–101.
[61] Tanaka E. A nonproportional parameter and a cyclic viscoelastic constitutive model taking into account amplitude dependences and memory effects of isotropic hardening. Eur J Mech A Solids 1994;13:155–73.
[62] Zhu Y, Kang G, Kan Q, Bruhns OT, Liu Y. Thermo-mechanically coupled cyclic elasto-viscoplastic constitutive model of metals: Theory and application. Int J Plast 2016;79:111–52.
[63] Jiang Y, Sehitoglu H. Modeling of cyclic ratchetting plasticity, Part I: Development of constitutive relations. J Appl Mech 1996;63:720–5.
[64] Nitta A, Ogata T, Kuwabara K. Fracture mechanisms and life assessment under high-strain biaxial cyclic loading of type 304 stainless steel. Fatigue Fract Eng Mater Struct 1989;12:77–92.
[65] Yang S, Yang L, Wang Y. Determining the fatigue parameters in total strain life equation of a material based on monotonic tensile mechanical properties. Eng Fract Mech 2020;226:106866.
[66] Jiang Y, Kurath P. Nonproportional cyclic deformation: Critical experiments and analytical modeling. Int J Plast 1997;13(8–9):743–63.
[67] Park J-H, Song J-H. Detailed evaluation of methods for estimation of fatigue properties. Int J Fatigue 1995;17(5):365–73.
[68] Jeon W-S, Song J-H. An expert system for estimation of fatigue properties of metallic materials. Int J Fatigue 2002;24(6):685–98.
[69] Park J-H, Song J-H. New estimation method of fatigue properties of aluminum alloys. J Eng Mater Technol ASME 2003;125.